Table 1
MiaPaCa-2 cell cDNAs isolated from 3T3 transformants

Clone ID #	Gene symbol	GenBank No.	Presence of entire ORF
1	CGI-152	NM_020410	Yes
2	RAB28	NM_004249	Yes
3	MRPL43	NM_032112	Yes
4	LTBR	NM_002342	No
5	UBQLN1	NM_013438	Yes
6	TBC1D2	NM_018421	Yes
7	FKBP10	NM_021939	Yes
8	HCCA2	NM_053005	Yes
9	Unknown	AK123415	ND
10	KRAS2	NM_004985	Yes
11	STK11IP	NM_052902	Yes
12	Unknown	AA627562	ND
13	PFKP	NM_002627	Yes

ORF, open reading frame; ND, not determined.

extensively investigated [3], little is known of such activity for *LTBR*. We thus focused on *LTBR* for further analysis.

Identification of a truncated form of LTBR

Although the nucleotide sequence of both ends of our LTBR cDNA was identical to that of human *LTBR*, the size of our cDNA (1452 bp) was smaller than that (2136 bp) of the full-length cDNA previously described. We thus determined the complete nucleotide sequence of our cDNA, revealing that it starts at nucleotide position 685 of the reported sequence (NM_002342). The longest open reading frame in our cDNA begins at amino acid position 221 and ends at position 435 of the previously described LTBR protein; it therefore encodes a predicted protein of 215 amino acids with a calculated molecular mass of 22,692 Da (Fig. 2). Given that the nucleotide sequence surrounding the putative translation start site of our cDNA matches the consensus Kozak motif, the corresponding mRNA likely produces this NH_2-terminally truncated form of LTBR, which is hereafter referred to as short-type LTBR.

5′-RACE analysis of LTBR mRNA

To confirm the presence of an mRNA encoding short-type LTBR in MiaPaCa-2 cells, we performed 5′-RACE to determine the 5′ ends of LTBR mRNAs. The first strand of LTBR cDNAs was generated with an LTBR-specific reverse transcription (RT) primer (Fig. 2) from RNA isolated from MiaPaCa-2 cells. Poly(A) was added to the 3′ end of the cDNAs, which were then subjected to nested PCR in order to amplify the 5′ ends. PCR products (ranging from a few hundred to 2000 bp) were detected only when reverse transcriptase was included in the procedure (Fig. 3A), indicating that the products were synthesized from cDNA, not from genomic DNA. The nucleotide sequence of 96 randomly chosen PCR products was determined. Sixty-eight of the 96 products matched the LTBR cDNA sequence and the positions of their 5′ ends are indicated in Fig. 3B. Transcription of most of the mRNAs corresponding to these PCR products was initiated in the region immediately upstream of the translation start site for short-type LTBR, indicating the existence of multiple mRNAs for this truncated protein in vivo.

Confirmation of transforming activity of short-type LTBR

To confirm the transforming activity of short-type LTBR, we examined its effect on anchorage-independent growth of 3T3 cells in soft agar. Whereas cells infected with an empty virus did not grow in soft agar, those infected with a virus encoding short-type LTBR formed multiple foci in repeated experiments (Fig. 4A). In addition, 3T3 cells expressing activated *KRAS2* readily grew in the agar.

We also injected the infected cells into nude mice. Tumors formed at all ($n = 10$) sites injected with 3T3 cells expressing short-type LTBR (Fig. 4B). Again, 3T3 cells expressing activated *KRAS2* also generated tumors at a high frequency, whereas those infected with the empty virus did not induce tumor formation. Together, these results thus confirmed that short-type LTBR possesses transforming activity.

Transforming activity of wild-type LTBR

To determine whether the full-length (435-amino acid) LTBR protein also possesses oncogenic potential, we performed the focus formation assay and in vivo tumorigenicity assay with a recombinant retrovirus encoding the wild-type

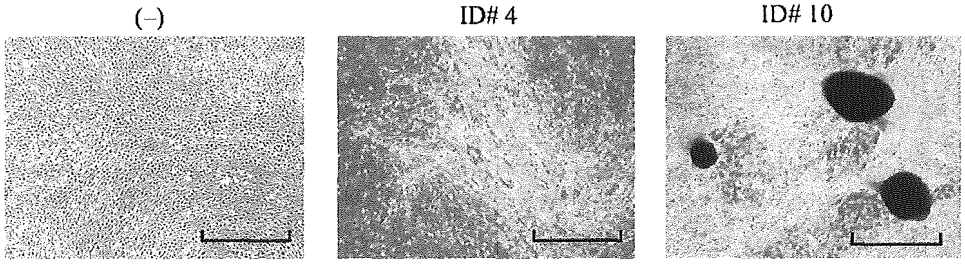

Fig. 1. Identification of transforming genes of MiaPaCa-2 cells. Mouse 3T3 cells were infected with an empty retrovirus (–) or with recombinant retroviruses harboring cDNAs corresponding to library clones ID #4 (short-type LTBR) or ID #10 (KRAS2). The cells were photographed after culture for 2 weeks. Scale bars, 1 mm.

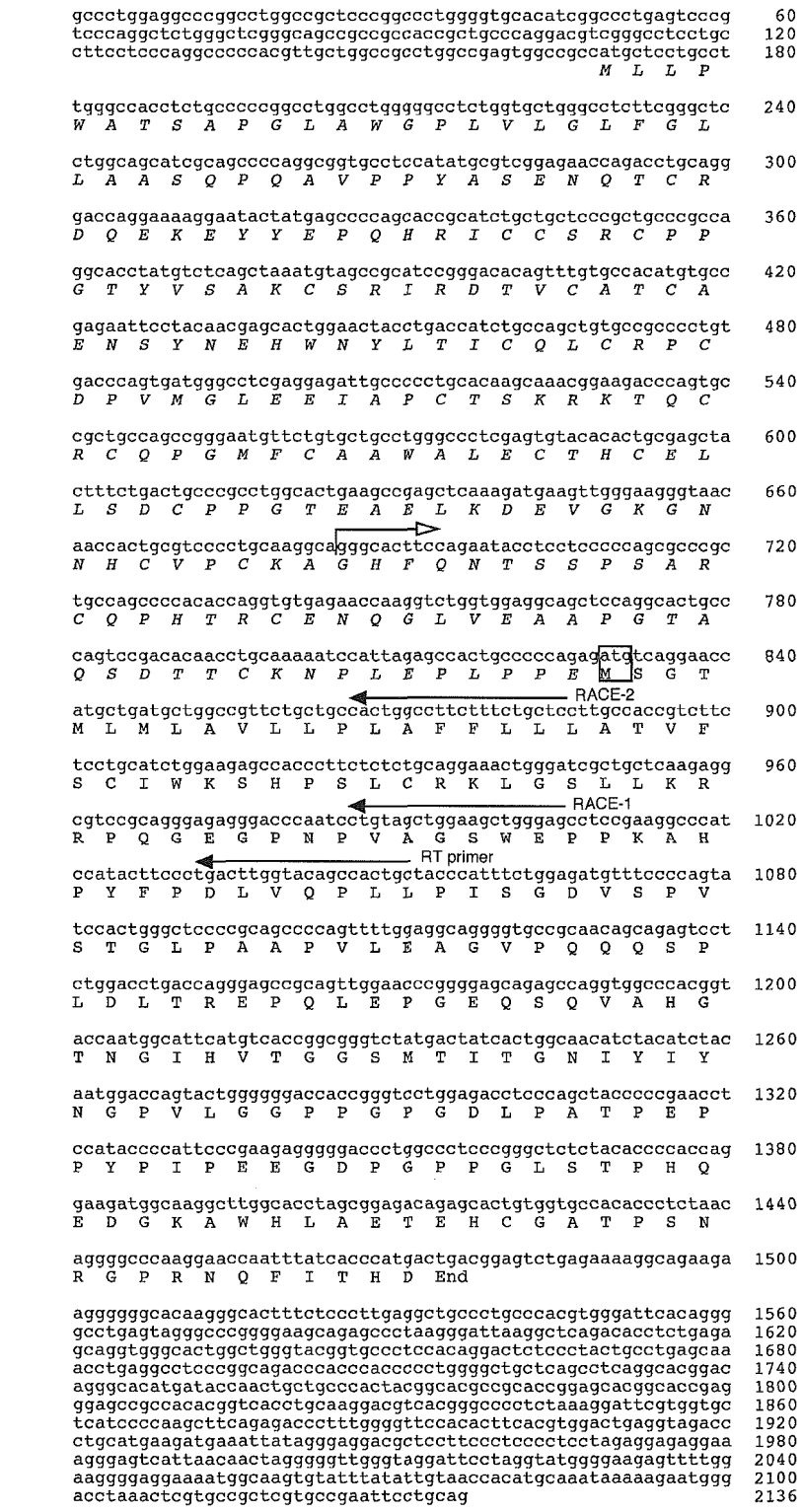

Fig. 2. Characterization of an LTBR cDNA isolated by screening for transformation activity. Amino acid residues of the full-length LTBR protein are aligned with the previously determined nucleotide sequence of LTBR cDNA (NM_002342). The cDNA isolated in the present study begins at nucleotide position 685 (open arrow) of the reported cDNA. The putative translation start site for the truncated (short-type) LTBR protein is boxed. The positions of primers used for 5′-RACE are indicated by closed arrows.

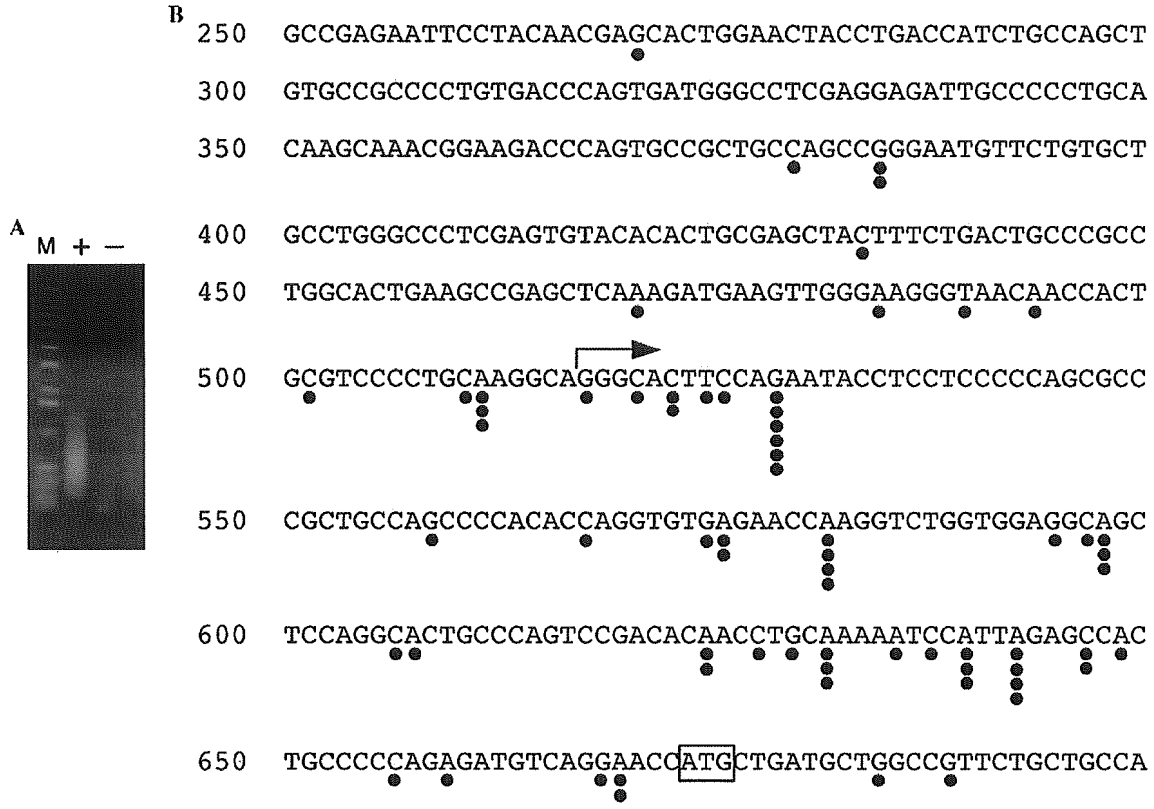

Fig. 3. 5′-RACE analysis of LTBR cDNA. (A) Total RNA of MiaPaCa-2 cells was incubated with the LTBR-specific RT primer in the presence (+) or absence (−) of reverse transcriptase, and resulting cDNA was subjected to PCR-based 5′-RACE. The PCR products were fractionated by electrophoresis through a 1.8% agarose gel and stained with ethidium bromide. Lane M, 1-kb DNA ladder. (**B**) The positions of the 5′ ends of 5′-RACE products are indicated by closed circles in alignment with the reported LTBR cDNA sequence. Numbers on the left indicate nucleotide positions relative to the translation initiation site of the full-length (wild-type) cDNA. The arrow indicates the 5′ end of the cDNA isolated by retroviral screening in the present study; the putative translation start codon of this cDNA is boxed.

human protein. The infected cells generated both transformed foci in vitro and tumors in nude mice (Fig. 5).

Discussion

In the present study, we constructed a retroviral cDNA expression library for a PDC cell line. Given that 80% (24/30) of the viral plasmids contained cDNA inserts and that the overall clone number was >1 million, this library should represent most of the mRNAs in MiaPaCa-2 cells. We infected 3T3 mouse fibroblasts with this recombinant library to screen for transforming genes with a focus formation assay. This screen identified *KRAS2* with an activating mutation as a transforming gene of MiaPaCa-2 cells, supporting the fidelity of our approach.

Our screen also identified a transforming cDNA that encodes an NH_2-terminally truncated form of LTBR. 5′-RACE analysis revealed the existence of mRNAs for this short-type LTBR in MiaPaCa-2 cells, and retrovirus-mediated expression of the isolated cDNA in 3T3 cells conferred the ability to grow in soft agar in vitro as well as the ability to form tumors in vivo.

LTBR belongs to the tumor necrosis factor (TNF) receptor superfamily [9] and binds two functional ligands, lymphotoxin-$\alpha 1\beta 2$ and LIGHT [10,11]. LTBR is expressed by many cell types (but not by lymphocytes), whereas expression of the LTBR ligands is restricted to activated lymphocytes [11]. Signaling by LTBR is important in the development of lymphoid tissue and in generation of adaptive humoral immune responses [12,13]. In general, LTBR function is thought to be linked to apoptosis. Indeed, activation of LTBR by its endogenous ligands or by anti-receptor antibodies triggers the death of various tumor cell lines [14,15]. Activation of the LIGHT-LTBR signaling pathway in tumor cells also induces marked chemokine-dependent recruitment of T cells to tumors, resulting in the rejection of established tumor cells [16].

LTBR activation has also been linked to tumor development, however. Its activation in fibrosarcoma cells thus induces angiogenesis and tumor growth by triggering the release of macrophage inflammatory protein-2, an angiogenic CXC chemokine [17]. Although oncogenic potential has not previously been demonstrated for LTBR, our data now show that both the full-length and truncated forms of this protein possess transforming activity even in the absence of exogenous cognate ligands. A high level of expression of LTBR conferred by the retroviral long terminal repeat in our experiments might have resulted in self-oligomerization

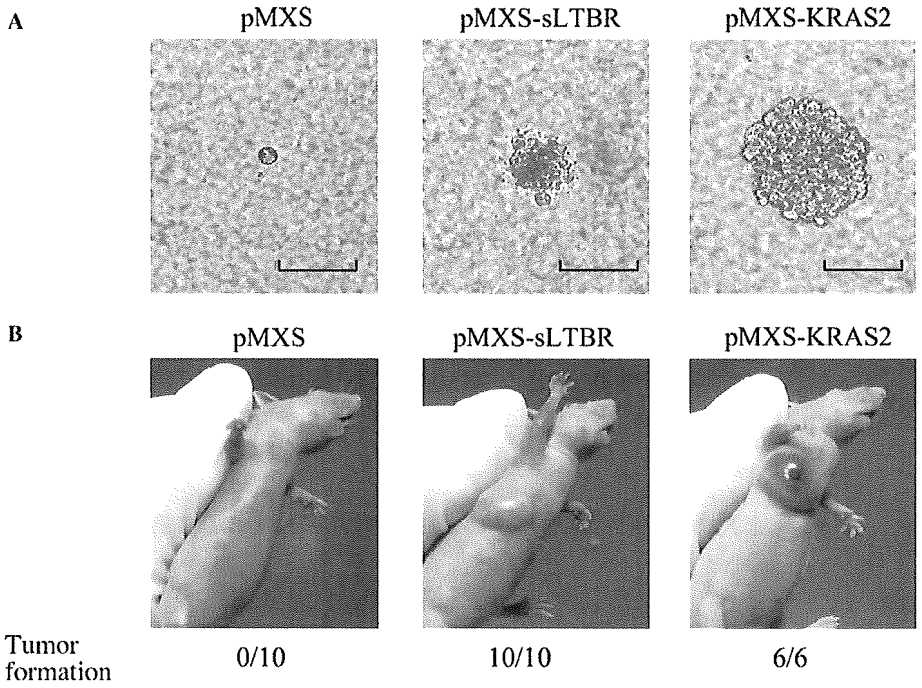

Fig. 4. Transforming activity of short-type LTBR. (A) Focus formation assay. 3T3 cells infected either with empty retrovirus (pMXS) or with retroviruses encoding short-type LTBR (pMXS-sLTBR) or activated KRAS2 (pMXS-KRAS2) were seeded into soft agar and incubated for 2 weeks. Scale bars, 100 μm. (B) Tumorigenicity assay. Cells infected as in (A) were injected into the shoulder of nude mice and tumor formation was examined after 3 weeks. The frequency of tumor formation determined is indicated.

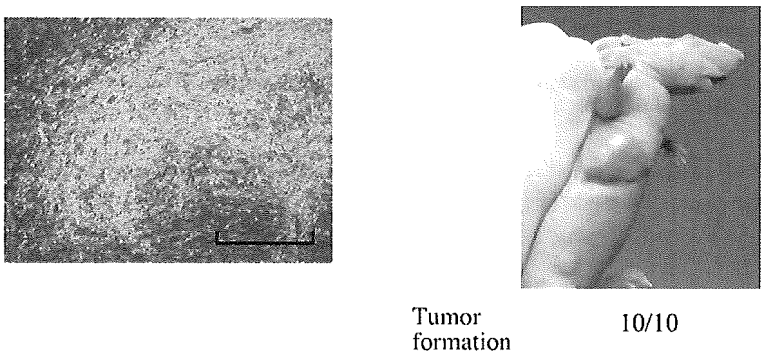

Fig. 5. Transforming activity of full-length LTBR. The transforming activity of a retroviral vector encoding full-length (wild-type) LTBR was evaluated by the focus formation assay (left) or the in vivo tumorigenicity assay (right). Scale bar, 1 mm.

of the protein. It is thus likely that LTBR exerts its oncogenic function in a tissue- and context-dependent manner. As shown here for PDC, it will be important to determine whether LTBR also contributes to the mechanism of transformation in other human malignancies.

Acknowledgments

This work was supported in part by a grant for Third-Term Comprehensive Control Research for Cancer from the Ministry of Health, Labor, and Welfare of Japan as well as by a grant for "High-Tech Research Center" Project for Private Universities: Matching Fund Subsidy (2002–2006) from the Ministry of Education, Culture, Sports, Science and Technology of Japan.

References

[1] S. Rosewicz, B. Wiedenmann, Pancreatic carcinoma, Lancet 349 (1997) 485–489.
[2] P.C. Bornman, I.J. Beckingham, Pancreatic tumours, Br. Med. J. 322 (2001) 721–723.
[3] M. Tada, M. Omata, M. Ohto, Clinical application of ras gene mutation for diagnosis of pancreatic adenocarcinoma, Gastroenterology 100 (1991) 233–238.
[4] S.R. Bramhall, The use of molecular technology in the differentiation of pancreatic cancer and chronic pancreatitis, Int. J. Pancreatol. 23 (1998) 83–100.

[5] G. Schneider, J.T. Siveke, F. Eckel, R.M. Schmid, Pancreatic cancer: basic and clinical aspects, Gastroenterology 128 (2005) 1606–1625.
[6] A. Yanagisawa, K. Ohtake, K. Ohashi, M. Hori, T. Kitagawa, H. Sugano, Y. Kato, Frequent c-Ki-ras oncogene activation in mucous cell hyperplasias of pancreas suffering from chronic inflammation, Cancer Res. 53 (1993) 953–956.
[7] S.A. Aaronson, Growth factors and cancer, Science 254 (1991) 1146–1153.
[8] M.A. Frohman, M.K. Dush, G.R. Martin, Rapid production of full-length cDNAs from rare transcripts: amplification using a single gene-specific oligonucleotide primer, Proc. Natl. Acad. Sci. USA 85 (1988) 8998–9002.
[9] P.D. Crowe, T.L. VanArsdale, B.N. Walter, C.F. Ware, C. Hession, B. Ehrenfels, J.L. Browning, W.S. Din, R.G. Goodwin, C.A. Smith, A lymphotoxin-β-specific receptor, Science 264 (1994) 707–710.
[10] J.L. Browning, I.D. Sizing, P. Lawton, P.R. Bourdon, P.D. Rennert, G.R. Majeau, C.M. Ambrose, C. Hession, K. Miatkowski, D.A. Griffiths, A. Ngam-ek, W. Meier, C.D. Benjamin, P.S. Hochman, Characterization of lymphotoxin-αβ complexes on the surface of mouse lymphocytes, J. Immunol. 159 (1997) 3288–3298.
[11] W.R. Force, B.N. Walter, C. Hession, R. Tizard, C.A. Kozak, J.L. Browning, C.F. Ware, Mouse lymphotoxin-β receptor. Molecular genetics, ligand binding, and expression, J. Immunol. 155 (1995) 5280–5288.
[12] A. Futterer, K. Mink, A. Luz, M.H. Kosco-Vilbois, K. Pfeffer, The lymphotoxin β receptor controls organogenesis and affinity maturation in peripheral lymphoid tissues, Immunity 9 (1998) 59–70.
[13] R.M. Locksley, N. Killeen, M.J. Lenardo, The TNF and TNF receptor superfamilies: integrating mammalian biology, Cell 104 (2001) 487–501.
[14] J.L. Browning, K. Miatkowski, I. Sizing, D. Griffiths, M. Zafari, C.D. Benjamin, W. Meier, F. Mackay, Signaling through the lymphotoxin β receptor induces the death of some adenocarcinoma tumor lines, J. Exp. Med. 183 (1996) 867–878.
[15] I.A. Rooney, K.D. Butrovich, A.A. Glass, S. Borboroglu, C.A. Benedict, J.C. Whitbeck, G.H. Cohen, R.J. Eisenberg, C.F. Ware, The lymphotoxin-β receptor is necessary and sufficient for LIGHT-mediated apoptosis of tumor cells, J. Biol. Chem. 275 (2000) 14307–14315.
[16] P. Yu, Y. Lee, W. Liu, R.K. Chin, J. Wang, Y. Wang, A. Schietinger, M. Philip, H. Schreiber, Y.X. Fu, Priming of naive T cells inside tumors leads to eradication of established tumors, Nat. Immunol. 5 (2004) 141–149.
[17] T. Hehlgans, B. Stoelcker, P. Stopfer, P. Muller, G. Cernaianu, M. Guba, M. Steinbauer, S.A. Nedospasov, K. Pfeffer, D.N. Mannel, Lymphotoxin-β receptor immune interaction promotes tumor growth by inducing angiogenesis, Cancer Res. 62 (2002) 4034–4040.

Experimental trial for diagnosis of pancreatic ductal carcinoma based on gene expression profiles of pancreatic ductal cells

Madoka Ishikawa,[1] Koji Yoshida,[2] Yoshihiro Yamashita,[1] Jun Ota,[1,3] Shuji Takada,[1] Hiroyuki Kisanuki,[1] Koji Koinuma,[1] Young Lim Choi,[1] Ruri Kaneda,[1] Toshiyasu Iwao,[4] Kiichi Tamada,[5] Kentaro Sugano[5] and Hiroyuki Mano[1,3,6]

[1]Division of Functional Genomics, Jichi Medical School, 3311-1 Yakushiji, Kawachi-gun, Tochigi 329-0498; [2]Department of Medicine, Kawasaki Medical School, Okayama 701-0192; [3]CREST, Japan Science and Technology Agency, 4-1-8, Honcho, Kawaguchi-shi, Saitama 332-0012; [4]Gastroenterological Center, Aizu Central Hospital, 1-1 Tsuruga-machi, Aizu-Wakamatsu, Fukushima 956-8611; and [5]Division of Gastroenterology, Jichi Medical School, 3311-1 Yakushiji, Kawachi-machi, Kawachi, Tochigi 329-0498, Japan

(Received November 18, 2004/Revised April 25, 2005/Accepted April 27, 2005/Online Publication July 22, 2005)

Pancreatic ductal carcinoma (PDC) remains one of the most intractable human malignancies, mainly because of the lack of sensitive detection methods. Although gene expression profiling by DNA microarray analysis is a promising tool for the development of such detection systems, a simple comparison of pancreatic tissues may yield misleading data that reflect only differences in cellular composition. To directly compare PDC cells with normal pancreatic ductal cells, we purified MUC1-positive epithelial cells from the pancreatic juices of 25 individuals with a normal pancreas and 24 patients with PDC. The gene expression profiles of these 49 specimens were determined with DNA microarrays containing >44 000 probe sets. Application of both Welch's analysis of variance and effect size-based selection to the expression data resulted in the identification of 21 probe sets corresponding to 20 genes whose expression was highly associated with clinical diagnosis. Furthermore, correspondence analysis and 3-D projection with these probe sets resulted in separation of the transcriptomes of pancreatic ductal cells into distinct but overlapping spaces corresponding to the two clinical classes. To establish an accurate transcriptome-based diagnosis system for PDC, we applied supervised class prediction algorithms to our large data set. With the expression profiles of only five predictor genes, the weighted vote method diagnosed the class of samples with an accuracy of 81.6%. Microarray analysis with purified pancreatic ductal cells has thus provided a basis for the development of a sensitive method for the detection of PDC. (*Cancer Sci* 2005; 96: 387–393)

Pancreatic ductal carcinoma (PDC), arising from the pancreatic ductal cells, accounts for more than 85% of all pancreatic malignancies, and is one of the most intractable malignancies in humans.[1,2] Effective therapy for PDC is hampered by the lack of specific clinical symptoms, with a 5-year survival rate of only 20 to 30%. An increase in the serum concentration of the protein CA19-9 is a reliable marker for PDC, but such an increase is only apparent in the advanced stages of disease.[3] Furthermore, although activating mutations of the *KRAS* oncogene have been detected in PDC cells, such mutations are also associated with other conditions, including chronic pancreatitis.[4,5]

DNA microarray analysis allows the simultaneous monitoring of the expression level of thousands of genes[6,7] and is therefore a potentially suitable approach for the identification of novel molecular markers for detection of the early stages of PDC. However, caution is warranted in simple comparisons between normal and cancerous pancreatic tissues. Because normal pancreatic tissue is composed mostly of exocrine and endocrine cells, and cancerous pancreatic tissue consists mostly of tumor cells that arise from ductal epithelial cells, a simple comparison between these two tissues tends to identify cell lineage-dependent gene expression differences.[8]

To minimize such misleading data that are attributable to population-shift effects, we have set up a depository for pancreatic ductal cells purified from pancreatic juice collected from patients during endoscopic retrograde cholangiopancreatography (ERCP). Comparison of such pancreatic ductal cell preparations between control individuals and PDC patients by DNA microarray analysis has the potential to identify specific gene markers for the latter. Indeed, an initial screening of a limited number of samples (from three individuals with a normal pancreas and six with PDC) with a DNA microarray of 3456 genes yielded candidates for new PDC marker genes.[8]

We have now expanded this project by using a larger number of specimens: 25 from individuals with a normal pancreas and 24 from PDC patients. Each purified preparation of pancreatic ductal cells was subjected to microarray experiments with Affymetrix HGU133 A&B GeneChips, which contain >44 000 probe sets corresponding to ~33 000 human genes. The application of sophisticated bioinformatics techniques to this large data set (a total of 2 156 000 data points) resulted in the establishment of an algorithm to differentiate transformed ductal cells from normal ones.

Materials and Methods

Preparation of pancreatic ductal cells. The study subjects comprised individuals who underwent ERCP and collection of pancreatic juice for cytological examination. The subjects gave informed consent and the study was approved by the institutional review board of Jichi Medical School. Diagnosis of patients was confirmed on the basis of the combination of results obtained by ERCP, cytological examination of pancreatic juice, abdominal computed tomography, and measurement of the serum concentration of CA19-9, as well as of follow-up observations. Approximately one-third of each specimen of pancreatic juice was used to purify MUC1$^+$ ductal cells.[9]

Cells were collected from the pancreatic juice by centrifugation and were resuspended in 1 mL of MACS binding buffer (150 mM NaCl, 20 mM sodium phosphate [pH 7.4], 3% fetal bovine serum, 2 mM ethylenediamine tetraacetic acid). They were then incubated for 30 min at 4°C with 0.5 μg of a mouse

[6]To whom correspondence should be addressed. E-mail: hmano@jichi.ac.jp

Abbreviations: ACTB, β-actin; EPPK1, epiplakin 1; ERCP, endoscopic retrograde cholangiopancreatography; H2BFB, H2B histone family, member B; KNN, *k* nearest neighbor; NRCAM, neuronal cell adhesion molecule; PCR, polymerase chain reaction; PDC, pancreatic ductal carcinoma; PLOD2, procollagen-lysine, 2-oxoglutarate 5-dioxygenase 2; RASAL2, RAS protein activator-like 2; SCGB3A1, secretoglobin, family 3A, member 1; SST, somatostatin; WV, weighted vote.

 doi:10.1111/j.1349-7006.2005.00064.x

monoclonal antibody to MUC1 (Novocastra Laboratories, Newcastle upon Tyne, UK), washed with MACS binding buffer, and mixed with MACS MicroBeads conjugated with antibodies to mouse immunoglobulin G (Miltenyi Biotec, Auburn, CA, USA). The resulting mixture was subjected to chromatography on a miniMACS magnetic cell separation column (Miltenyi Biotec), and the eluted MUC1$^+$ cells were divided into portions and stored at −80°C. Portions of the unfractionated cells as well as the isolated MUC1$^+$ cells of each individual were stained with Wright–Giemsa solution to examine the purity of the ductal cell-enriched fractions.

Microarray experiments. Total RNA was extracted from the MUC1$^+$ cell preparations with the use of an RNeasy Mini column and RNase-free DNase (Qiagen, Valencia, CA, USA) and was subjected to two rounds of mRNA amplification with T7 RNA polymerase.[10] The high fidelity of the amplification step has been demonstrated previously.[11] One microgram of the amplified cRNA was then converted to double-stranded cDNA by PowerScript reverse transcriptase (BD Biosciences Clontech, Palo Alto, CA, USA), and the cDNA was used to prepare biotin-labeled cRNA with an ENZO BioArray Transcript Labeling Kit (Affymetrix, Santa Clara, CA, USA). Hybridization of the labeled cRNA with GeneChip HGU133 A&B microarrays, which contain >44 000 probe sets, was performed with the GeneChip system (Affymetrix). The mean expression intensity of the internal positive control probe sets[12] was set to 500 arbitrary units (U) in each hybridization, and the fluorescence intensity of each test gene was normalized accordingly. All normalized array data are available at the Gene Expression Omnibus web site (http://www.ncbi.nlm.nih.gov/geo) under the accession number GSE1542.

Statistical analysis. Hierarchical clustering of the data set, Welch's analysis of variance (ANOVA), and k nearest neighbor (KNN) method-based class prediction were performed with GeneSpring 6.2 software (Silicon Genetics, Redwood, CA). The weighted vote (WV) method[13] was performed with GeneCluster 2.1.7.[14] Correspondence analysis[15] for all genes showing a significant difference in expression was performed by using ViSta software.[16] Each sample was plotted in three dimensions based on the coordinates obtained from the correspondence analysis. With the exception of the effect-size selection, in which linear values were used for calculation, all normalized expression values were transformed to logarithms prior to analyses.

Real-time PCR analysis. Portions of nonamplified cDNA were subjected to PCR with a QuantiTect SYBR Green PCR Kit (Qiagen). The amplification protocol comprised incubations at 94°C for 15 s, 57°C for 30 s, and 72°C for 60 s. Incorporation of the SYBR Green dye into PCR products was monitored in real time with an ABI PRISM 7900 HT sequence detection system (PE Applied Biosystems, Foster City, CA, USA), thereby allowing determination of the threshold cycle (C_T) at which exponential amplification of products begins. The C_T values for cDNA corresponding to the β-actin gene (*ACTB*) and to the target genes were used to calculate the abundance of target gene mRNA relative to that of *ACTB* mRNA. The oligonucleotide primers for PCR were as follows: 5′-CCATCATGAAGTGTGACGTGG-3′ and 5′-GTCCGCCTAGAAGCATTTGCG-3′ for *ACTB*, 5′-CCCGTGAACCACCTCATAG-3′ and 5′-AGCGTCTTGTCCTCAGGTGTA-3′ for the secretoglobin, family 3A, member 1 gene (*SCGB3A1*), and 5′-GATGAAATGAGGCTTGAGCTG-3′ and 5′-GTTTCTAATGCAAGGGTCTCG-3′ for the somatostatin gene (*SST*).

Results

Transcriptome of pancreatic ductal cells. As demonstrated previously, affinity purification with antibodies to MUC1 yielded an apparently homogeneous preparation of pancreatic ductal cells.[8] With this approach, we purified pancreatic ductal cell specimens from 25 individuals with a normal pancreas and 24 patients with PDC. Clinical characteristics for the latter individuals are summarized in Table 1. All 49 specimens were each subjected to DNA microarray analysis with Affymetrix HGU133 A&B GeneChips, which contain >44 000 probe sets.

Table 1. Clinical characteristics of patients with PDC

Patient	Age (years)	Sex	Cytological examination	Atypical cell proportion*	Clinical stage†
ID073	74	Male	V	H	IVa
ID086	72	Female	IV	M	IVa
ID088	65	Male	V	L	IVb
ID089	70	Female	III	L	III
ID090	72	Male	III	L	IVa
ID095	85	Female	III	L	0
ID096	76	Female	IV	L	IVa
ID098	61	Female	IV	L	IVa
ID103	65	Male	V	H	IVb
ID117	76	Female	IV	L	IVa
ID119	73	Female	V	L	IVa
ID120	70	Female	III	M	0
ID125	75	Male	II	L	I
ID131	67	Female	II	L	IVa
ID142	69	Male	III	H	I
ID147	51	Male	V	L	IVb
ID202	56	Female	III	M	IVa
ID203	73	Male	III	M	I
ID218	51	Male	III	L	0
ID224	71	Male	V	L	IVa
ID225	50	Female	III	L	IVa
ID227	65	Male	I	L	III
ID229	60	Female	IV	M	IVa
ID234	71	Male	III	L	IVa

*Isolated ductal cells contained <20% (L), 20–40% (M) or ≧ 40% (H) of atypical cells. †Clinical stage was determined according to the proposal of Isaji *et al.*[25]

For analysis of the gene expression data, we first set the condition that the expression level of a given probe set should receive the 'Present call' (from Microarray Suite 5.0 software) in at least 30% (n = 15) of the samples in order to exclude transcriptionally silent genes from the analysis. A total of 7778 probe sets fulfilled this selection criterion. Unsupervised two-way hierarchical clustering analysis[17] was then applied to the 49 specimens based on the expression profiles of these 7778 probe sets, generating a dendrogram in which the samples are clustered according to the similarity in expression pattern of the probe sets (Fig. 1). Although this dendrogram contained a large branch consisting mostly of PDC patients, normal and cancer specimens did not form separate, diagnosis-dependent branches. The transcriptome of virtually all expressed genes thus did not differ sufficiently between normal and cancerous ductal cells to allow diagnosis.

PDC-specific molecular signature. To capture a PDC-specific molecular signature, we next identified genes whose expression level differed significantly between the normal and cancerous ductal cells. Application of Welch's ANOVA ($P < 0.001$) for this purpose yielded 26 out of the 7778 probe sets examined. However, some of the probe sets thus identified had low absolute expression levels throughout the samples, even though the ratio of the expression levels between the two classes was relatively large. To eliminate such 'nearly silent' genes and to enrich genes whose expression level was markedly increased in at least one of the classes, we further selected those whose effect size (absolute difference in mean expression intensities)[18] between the two classes was ≧ 50 U.

 doi:10.1111/j.1349-7006.2005.00064.x

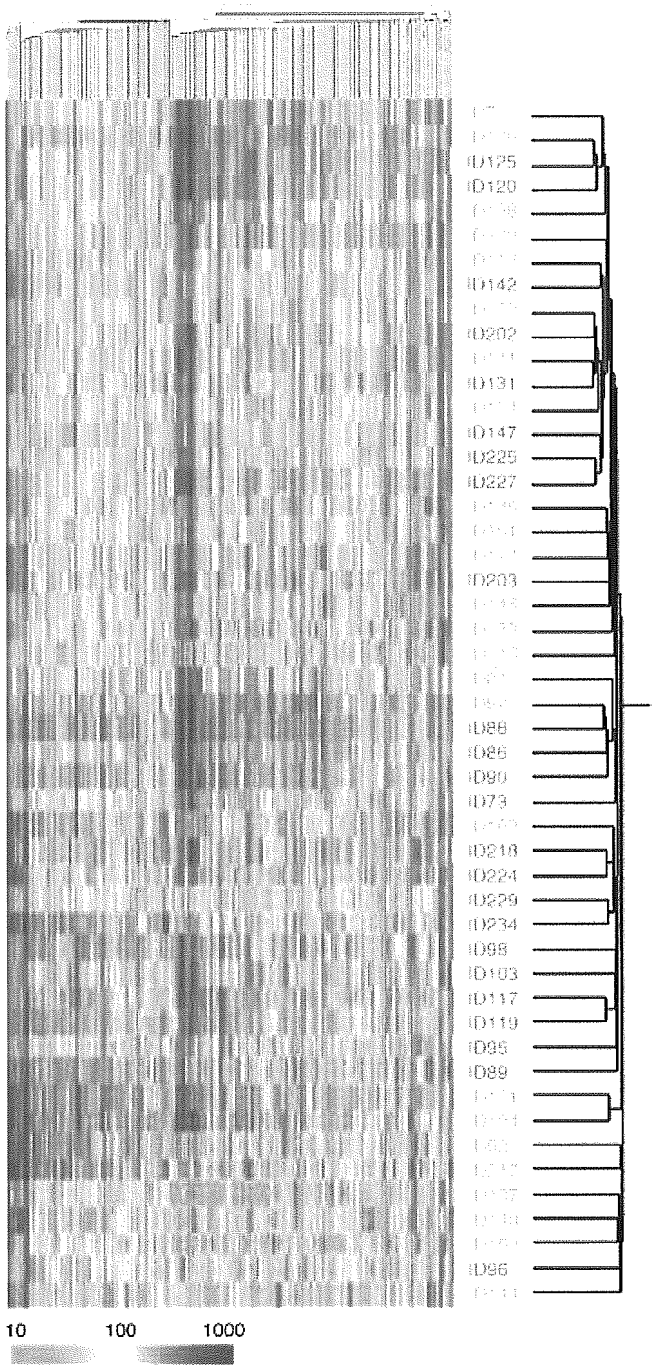

Fig. 1. Gene expression profiles of the purified pancreatic ductal cells. Hierarchical two-way clustering of the study subjects (normal ductal cell specimens [green] and PDC specimens [red]) was performed on the basis of the expression profiles of 7778 probe sets. Each column corresponds to a single probe set, and each row corresponds to a separate subject. The expression level of probe sets is color-coded according to the indicated scale.

With this approach, we identified 21 probe sets (corresponding to 20 independent genes) whose expression levels differed significantly between the two clinical conditions. Construction of a dendrogram for the expression profiles of these 21 probe sets revealed that the subjects were grouped into two major branches (Fig. 2a). Although each branch corresponded approximately to the two clinical classes, a few subjects were still misclassified in both branches. It was not clear, however, whether this failure to clearly separate the two clinical classes was due to an inadequacy of the separation power of the clustering method or to the heterogeneity of the samples within each clinical class. Furthermore, these results did not address whether normal and cancerous ductal cells are truly distinct from each other from the point of view of gene expression profiles.

To address these issues, we attempted to visualize the similarity or difference between the two classes. Correspondence analysis is a relatively new approach to the decomposition of multidimensional data.[15] It allows not only a low-dimensional projection of expression profiles for numerous genes, but also measurement both of the contribution of each gene to a given extracted dimension and of the contribution of each extracted dimension to the total complexity. Correspondence analysis of the expression data of the 21 probe sets shown in Fig. 2a reduced the number of dimensions from 21 to three. On the basis of the calculated 3-D coordinates for each sample, the specimens were then projected into a virtual space (Fig. 2b). Although most of the normal samples were positioned in a region of the space distant from that occupied by the PDC specimens, the two groups were not separated completely. Decomposition of the data set was thus not sufficiently effective to achieve a high accuracy in differential diagnosis.

Supervised class prediction. We next attempted class prediction by using two supervised algorithms. The WV method was recently developed to assign binary classes based on gene expression profiles.[13] A defined number of 'class predictor' genes whose expression contrasts the two classes most effectively are first selected in a training data set. A weighting factor, which reflects how well a gene is correlated with the class distinction, is also calculated for each gene. The expression levels of the class predictors are then quantitated in the test data set, and the 'prediction strength' is determined on the basis of the expression intensities and weighting factors of the predictors. The WV method has been successfully used to differentiate acute myeloid leukemia from acute lymphoid leukemia,[13] as well as diffuse large B cell lymphoma with poor prognosis from that with good prognosis.[19]

The KNN method, like the WV method, first involves the selection of a defined number of predictor genes. It then finds nearest neighbors to the classes based on a distance function for pairs of observations. The KNN method predicts the class of a given test sample based on the majority of votes among the nearest neighbors.[20]

To measure precisely the class prediction ability of these two methods, we performed a cross-validation trial for each with our data set: One sample was therefore set aside and the program was trained with the remaining 48 samples; the class of the withheld test sample was then predicted by the program, and the trial was repeated for each of the 49 samples to calculate the overall accuracy of the program.

For both WV and KNN methods, the cross-validation was performed with the 49 specimens and with different numbers of class predictor genes (n = 1 to 20, 30, 40, 50, 60, 70, 80, 90, or 100). Both methods had similar error rates, with the WV method having a slightly lower error rate than the KNN method (Fig. 3a). The best prediction accuracy (81.6%) was obtained by the WV method with five class predictor genes. In this cross-validation, different sets of five predictors were selected for each leave-one-out trial, with a total of 11 probe sets (corresponding to 10 genes) used as predictors. Two-way clustering of the expression profiles of these 11 probe sets yielded the dendrogram shown in Fig. 3b. It should be noted that two probe sets (DKFZp564I1922 and EPPK1) were selected as the predictors in all 49 leave-one-out trials.

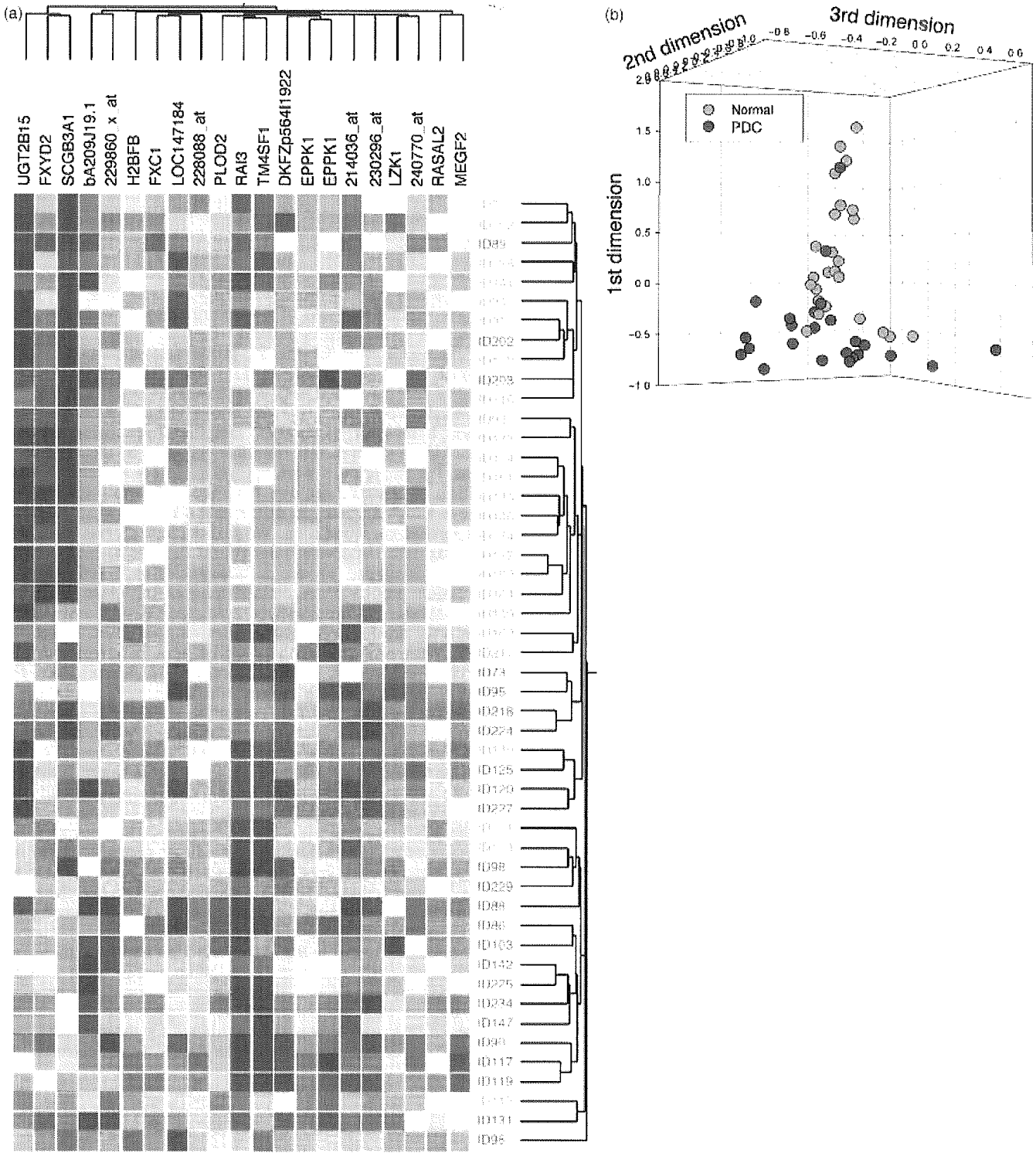

Fig. 2. Isolation of a PDC-specific molecular signature. (a) Dendrogram of the 21 probe sets whose expression level differed significantly (Welch's ANOVA, $P < 0.001$) with an effect size of ≧ 50 U between normal and cancerous specimens. Each row corresponds to a separate subject, and each column to a probe set whose expression is color-coded according to the scale in 1. Gene symbols are shown at the top; 229860_x_at, 228088_at, 214036_at, 230296_at, and 240770_at are expressed sequence tag IDs designated by Affymetrix. Detailed information on the genes and their expression levels is provided in Supplementary Information at the *Cancer Science* web site. (b) Correspondence analysis of the 21 probe sets identified three major dimensions in their expression profiles. Projection of the specimens into a virtual space with these three dimensions revealed that those from individuals with a normal pancreas and those from patients with PDC were partially separated.

 doi:10.1111/j.1349-7006.2005.00064.x

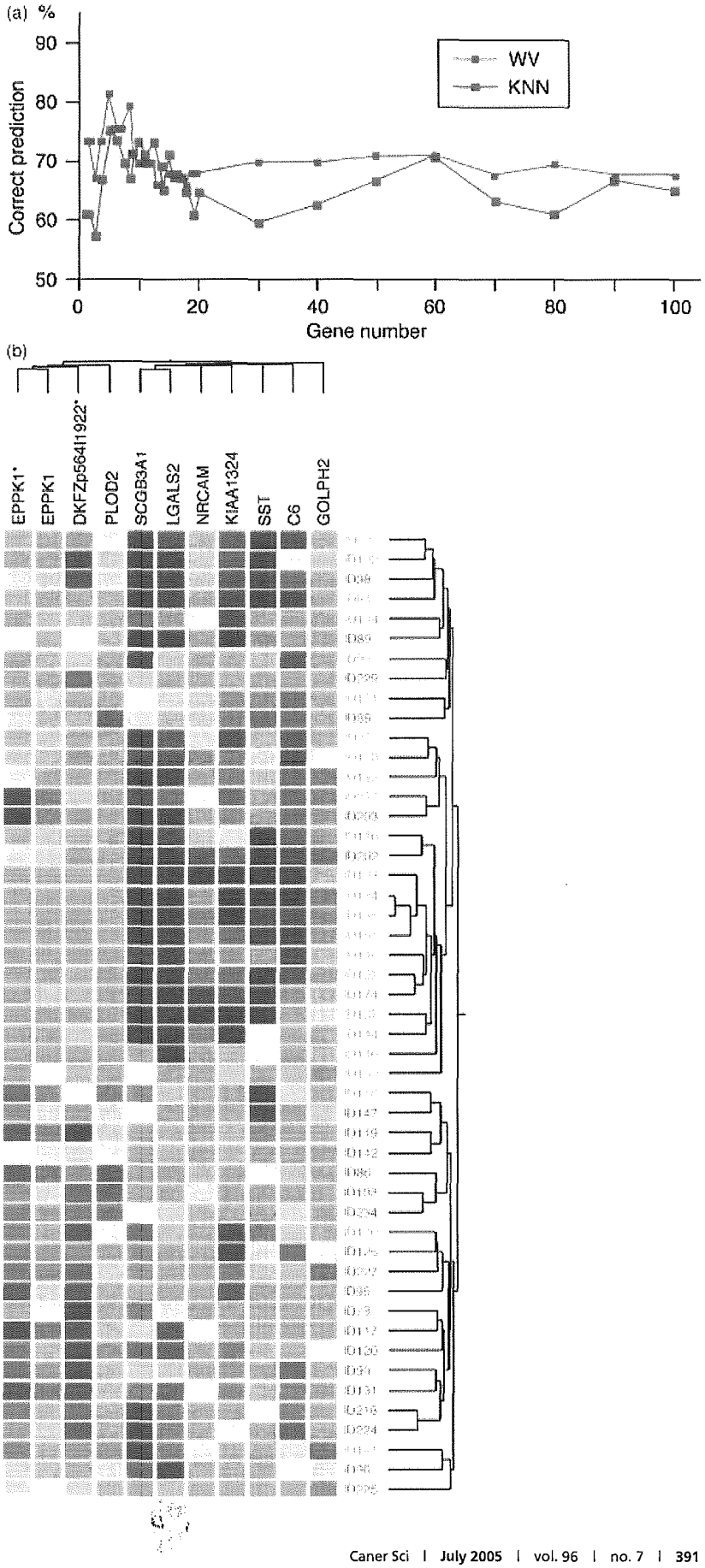

Fig. 3. Supervised class prediction. (a) Cross-validation trials for class prediction of normal or PDC specimens based on various numbers of predictor genes were performed with the WV or KNN methods. Correct prediction rate (%) is plotted for each trial. (b) Expression profiles of 11 probe sets identified by the WV method with five predictors. Samples are clustered according to the similarity in the expression pattern of the 11 probe sets. Asterisks indicate the two probe sets selected in all trials. Detailed information on the genes and their expression levels is provided in Supplementary Information at the *Cancer Science* web site.

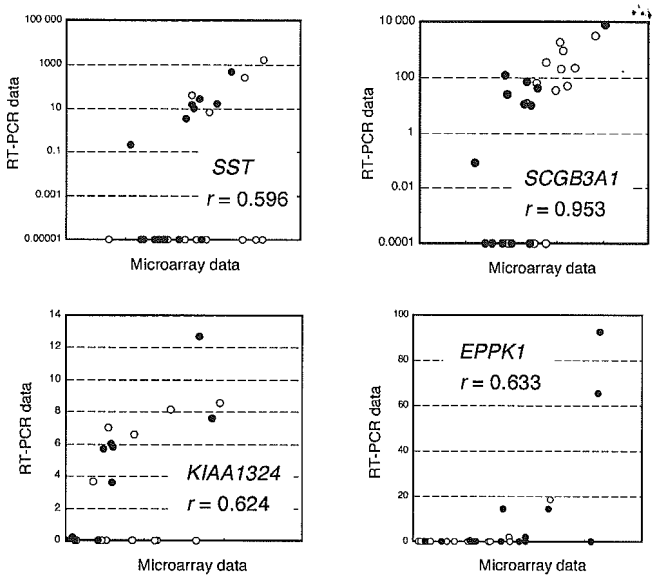

Fig. 4. Validation by reverse transcription and real-time PCR analysis of gene expression profiles obtained by microarray analysis. The relative amounts of mRNA corresponding to *SST, SCGB3A1, KIAA1324* or *EPPK1* in the MUC1+ cells derived from (○) healthy individuals or (●) patients with PDC were determined by reverse transcription and real-time PCR with *ACTB* transcripts as the internal standard. The resulting values are plotted against those obtained by microarray analysis. Pearson's correlation coefficient (*r*) values are provided for each comparison.

Confirmation of expression data. To confirm the gene expression profiles obtained by microarray analysis, we measured the mRNA levels of some genes by reverse transcription and quantitative real-time PCR analysis. The relative amounts of mRNA derived from the *SST* (GenBank accession number NM_001048) or *SCGB3A1* (GenBank accession number AA742697) genes, for example, determined by this latter approach were highly correlated with those quantitated by microarray analysis (Fig. 4).

Discussion

In the present study, we constructed the largest gene expression database available to date for pancreatic ductal cells. Our statistical approach to identify genes associated with a diagnosis of PDC resulted in the extraction of 21 probe sets, three of which were preferentially expressed in normal ductal cells and the remaining 18 were preferentially expressed in cancerous ductal cells. The latter group contained the genes for H2B histone family member B (*H2BFB*; GenBank accession number BC002842), RAS protein activator-like 2 (*RASAL2*; GenBank accession number NM_004841), procollagen-lysine, 2-oxoglutarate 5-dioxygenase 2 (*PLOD2*; GenBank accession number NM_000935), adlican (DKFZp564I1922; GenBank accession number AF245505), and epiplakin 1 (*EPPK1*; GenBank accession number AL137725). H2BFB functions as a linker histone in nucleosome compaction.[21] The increased expression of *H2BFB* in PDC cells therefore probably reflects the increased proliferation rate of these cells. RASAL2 shares a GTPase-activating protein (GAP)-related domain with members of the RAS-GAP family of proteins and is thought to contribute to the regulation of small GTP-binding proteins. *RASAL2* is localized within the prostate cancer susceptibility locus at chromosome 1q25[22], so an altered activity of the encoded protein might thus be directly linked to carcinogenesis.

The expression profile of these disease-associated genes was not, however, sufficient to separate the specimens into the normal or cancer class with a high accuracy. We therefore applied sophisticated algorithms in the supervised mode in an attempt to achieve this goal. In our trials of the WV and KNN methods with various numbers of predictor genes, the WV method trained with five genes gave the best result. The accuracy of correct diagnosis achieved (81.6%) is higher than that obtained by cytological examination of pancreatic juice.[23]

In the 'leave-one-out' trials for all 49 samples, a total of 11 probe sets were chosen by the WV algorithm as the class predictors. These probe sets corresponded to 10 genes, including those for EPPK1, DKFZp564I1922, PLOD2, SCGB3A1, SST, and neuronal cell adhesion molecule (*NRCAM*; GenBank accession number NM_005010). NRCAM belongs to the immunoglobulin (Ig) superfamily of proteins, contains multiple repeats of the Ig domain in its extracellular region, and is expressed at the surface of neuronal cells. The DKFZp564I1922 protein also contains 12 repeats of the Ig domain.[24] Increased expression of these Ig domain-containing proteins may thus be a specific property and a novel molecular marker of PDC.

Among the 10 genes used in the WV analysis, only two (those for EPPK1 and DKFZp564I1922) were chosen as predictors in all 49 trials. In addition, the Welch's ANOVA strategy and the WV method selected five probe sets in common, including two sets for EPPK1, one for SCGB3A1, one for PLOD2, and one for DKFZp564I1922.

Cytological examination revealed that, among the individuals with PDC in our study, 16 patients had <20% of atypical cells in the purified ductal cell specimens ('L' in Table 1), three patients had ≧40% of such cells ('H'), and the other five patients had 20–40% of such cells ('M'). We thus examined whether the proportion of atypical cells in the specimens affected the expression intensities of the selected genes. The expression levels of the genes in Fig. 2a was, for instance, compared by Student's *t*-test between the individuals in the L and M groups, and between those in the M and H groups. Surprisingly, none of the genes in Fig. 2a were differentially expressed in a significant manner between these groups (data not shown). Therefore, our microarray-based prediction scheme should be of clinical importance even for patients with pancreatic juice containing small amounts of cancer cells.

Our strategy to identify a PDC-specific gene expression profile for purified pancreatic ductal cells should provide the basis for several possible scenarios for the early detection of PDC in the clinical setting. One scenario would be a microarray-based diagnosis of PDC with a sophisticated algorithm for analysis of the expression of a limited number of genes (as demonstrated in the present study). A second scenario would require an extension of our project to isolate single gene markers specific to PDC; the expression of such genes should be negligible in non-cancerous cells but would be markedly increased in cancerous cells. Such PDC-specific single gene markers would be good candidates for the construction of a sensitive PCR-based detection system for PDC. A third scenario may involve the identification of soluble proteins among the products of PDC-specific genes that could be detected in the serum of patients. Further expansion of our gene expression database would probably facilitate the development of such detection systems for PDC, which would improve the long-term prognosis of individuals with this intractable disease.

Acknowledgments

This work was supported in part by a Grant-in-Aid for research on the Third Term Comprehensive Control Research for Cancer from the Ministry of Health, Labour, and Welfare of Japan, and by a grant from the Research Foundation for Community Medicine.

 doi:10.1111/j.1349-7006.2005.00064.x

References

1 Bomman PC, Beckingham IJ. Pancreatic tumours. *Br Med J* 2001; **322**: 721–3.
2 Rosewicz S, Wiedenmann B. Pancreatic carcinoma. *Lancet* 1997; **349**: 485–9.
3 Sawabu N, Watanabe H, Yamaguchi Y, Ohtsubo K, Motoo Y. Serum tumor markers and molecular biological diagnosis in pancreatic cancer. *Pancreas* 2004; **28**: 263–7.
4 Kondo H, Sugano K, Fukayama N *et al.* Detection of point mutations in the K-ras oncogene at codon 12 in pure pancreatic juice for diagnosis of pancreatic carcinoma. *Cancer* 1994; **73**: 1589–94.
5 Furuya N, Kawa S, Akamatsu T, Furihata K. Long-term follow-up of patients with chronic pancreatitis and K-ras gene mutation detected in pancreatic juice. *Gastroenterology* 1997; **113**: 593–8.
6 Schena M, Shalon D, Davis RW, Brown PO. Quantitative monitoring of gene expression patterns with a complementary DNA microarray. *Science* 1995; **270**: 467–70.
7 Duggan DJ, Bittner M, Chen Y, Meltzer P, Trent JM. Expression profiling using cDNA microarrays. *Nat Genet* 1999; **21**: 10–4.
8 Yoshida K, Ueno S, Iwao T *et al.* Screening of genes specifically activated in the pancreatic juice ductal cells from the patients with pancreatic ductal carcinoma. *Cancer Sci* 2003; **94**: 263–70.
9 Terada T, Ohta T, Sasaki M, Nakamura Y, Kim YS. Expression of MUC apomucins in normal pancreas and pancreatic tumours. *J Pathol* 1996; **180**: 160–5.
10 Van Gelder RN, von Zastrow ME, Yool A, Dement WC, Barchas JD, Eberwine JH. Amplified RNA synthesized from limited quantities of heterogeneous cDNA. *Proc Natl Acad Sci USA* 1990; **87**: 1663–7.
11 Oshima Y, Ueda M, Yamashita Y *et al.* DNA microarray analysis of hematopoietic stem cell-like fractions from individuals with the M2 subtype of acute myeloid leukemia. *Leukemia* 2003; **17**: 1990–7.
12 Affymetrix [web site on the Internet]. Support: Mask files. Available from URL: http://www.affymetrix.com/support/technical/mask_files.affx
13 Golub TR, Slonim DK, Tamayo P *et al.* Molecular classification of cancer: class discovery and class prediction by gene expression monitoring. *Science* 1999; **286**: 531–7.
14 Broad Institute [web site on the Internet]. GeneCluster 2.0. Available from URL: http://www.broad.mit.edu/cancer/software/genecluster2/gc2.html
15 Fellenberg K, Hauser NC, Brors B, Neutzner A, Hoheisel JD, Vingron M. Correspondence analysis applied to microarray data. *Proc Natl Acad Sci USA* 2001; **98**: 10781–6.
16 ViSta. [web site on the Internet]. ViSta: the visual statistics system. Available from URL: http://www.visualstats.org
17 Alon U, Barkai N, Notterman DA *et al.* Broad patterns of gene expression revealed by clustering analysis of tumor and normal colon tissues probed by oligonucleotide arrays. *Proc Natl Acad Sci USA* 1999; **96**: 6745–50.
18 Dhanasekaran SM, Barrette TR, Ghosh D *et al.* Delineation of prognostic biomarkers in prostate cancer. *Nature* 2001; **412**: 822–6.
19 Shipp MA, Ross KN, Tamayo P *et al.* Diffuse large B-cell lymphoma outcome prediction by gene-expression profiling and supervised machine learning. *Nat Med* 2002; **8**: 68–74.
20 Dudoit S, Fridlyand J, Speed TP. [pre-print PDF on the Internet]. Comparison of discrimination methods for the classification of tumors using gene expression data. Available from URL: http://www.stat.berkeley.edu/tech-reports/index.html
21 Albig W, Kardalinou E, Drabent B, Zimmer A, Doenecke D. Isolation and characterization of two human H1 histone genes within clusters of core histone genes. *Genomics* 1991; **10**: 940–8.
22 Noto S, Maeda T, Hattori S, Inazawa J, Imamura M, Asaka M, Hatakeyama M. A novel human RasGAP-like gene that maps within the prostate cancer susceptibility locus at chromosome 1q25. *FEBS Lett* 1998; **441**: 127–31.
23 Nakaizumi A, Tatsuta M, Uehara H *et al.* Cytologic examination of pure pancreatic juice in the diagnosis of pancreatic carcinoma. The endoscopic retrograde intraductal catheter aspiration cytologic technique. *Cancer* 1992; **70**: 2610–4.
24 Strausberg RL, Feingold EA, Grouse LH *et al.* Generation and initial analysis of more than 15 000 full-length human and mouse cDNA sequences. *Proc Natl Acad Sci USA* 2002; **99**: 16 899–903.
25 Isaji S, Kawarada Y, Umemoto S. Classification of pancreatic cancer. Comparison of Japanese and UICC classifications. *Pancreas* 2004; **28**: 231–4.

Supplementary Material

The following supplementary material is available for this article online:

Table S1. Annotation information and expression intensity data for the genes shown in Figure 2A.

Table S2. Annotation information and expression intensity data for the genes shown in Figure 3B.

Genome-Wide Screening for Target Regions of Histone Deacetylases in Cardiomyocytes

Ruri Kaneda, Shuichi Ueno, Yoshihiro Yamashita, Young Lim Choi, Koji Koinuma, Shuji Takada, Tomoaki Wada, Kazuyuki Shimada, Hiroyuki Mano

Abstract—The acetylation status of core histones in cardiomyocytes has been linked to the development of cardiac hypertrophy and heart failure. Little is known, however, of the genes affected by abnormal histone acetylation in such pathological conditions. We recently developed a genome-wide screening method, differential chromatin scanning (DCS), to isolate genomic fragments associated with histones subject to differential acetylation. We have now applied DCS to H9C2 rat embryonic cardiomyocytes incubated with or without trichostatin A (TSA), a specific inhibitor of histone deacetylase (HDAC) activity. About 200 genomic fragments were readily isolated by DCS on the basis of the preferential acetylation of associated histones in TSA-treated cells. Quantitation of the amount of DNA in chromatin immunoprecipitates prepared with antibodies to acetylated histone H3 revealed that 37 of 38 randomly chosen DCS clones were preferentially precipitated from the TSA-treated cells, thus verifying the high fidelity of DCS. Epigenetic regulation of DCS clones was further confirmed in cells treated with sodium butyrate, another HDAC inhibitor, as well as in cardiac myocytes isolated from neonatal rats. The mRNA level of 9 (39%) of 23 genes corresponding to DCS clones changed in parallel with the level of histone acetylation in H9C2 cells. Furthermore, a physiological hypertrophic stimulus, cardiotrophin-1, affected the acetylation level of histones associated with genomic regions corresponding to certain DCS clones. Our data thus establish a genome-wide profile of HDAC targets in cardiomyocytes, which should provide a basis for further investigations into the role of epigenetic modification in cardiac disorders. (***Circ Res.* 2005;97:210-218.**)

Key Words: epigenetics ■ histone acetylation ■ trichostatin A ■ cardiomyocyte

Epigenetic modification of chromatin includes methylation of genomic DNA as well as acetylation, methylation, and phosphorylation of histone proteins. Such epigenetic changes play important roles in the regulation of gene transcriptional activity associated with cell growth and differentiation as well as with organ development.[1–3] Acetylation of core histones is mediated by histone acetyltransferases (HATs) and, in many instances, results in relaxation of chromatin structure and transcriptional activation of associated genes.[4] Histone deacetylases (HDACs) counteract HAT activity by catalyzing the removal of acetyl moieties from lysine residues in histone tails, thereby inducing chromatin condensation and transcriptional repression.[5]

Regulation of histone acetylation has been linked to cardiac hypertrophy. The HAT activity of CREB-binding protein (CBP) and p300 is thus required for the induction of hypertrophic changes in cardiac muscle cells by phenylephrine.[6] Consistent with this observation, inhibition of HDAC activity results in an increase in the size of muscle cells.[7] Furthermore, HDACs of class II (HDAC-4, -5, -7, and -9) suppress cardiac hypertrophy in part by binding to and inhibiting the activity of myocyte enhancer factor 2 (MEF2).[8] In contrast, however, HDAC2 together with Hop was found to promote cardiac hypertrophy in vivo in a manner sensitive to systemic administration of the HDAC inhibitor trichostatin A (TSA).[9] Moreover, HDAC inhibitors prevent hypertrophy and sarcomere organization in cultured cardiac myocytes,[10] suggestive of a positive role for HDACs in cardiac hypertrophy.

These seemingly discrepant findings may be attributable either to differential actions of different classes of HDACs (and, possibly, of HATs) with regard to myocyte hypertrophy or to a dissociation between the deacetylase activity of HDACs and a prohypertrophic function.[8] Clarification of the role of HATs and HDACs in hypertrophy would be facilitated by identification of the genes targeted by these enzymes during the induction of hypertrophic changes. Little is known, however, of the genes regulated by HATs or HDACs in myocytes. Induction of the atrial natriuretic peptide (ANP) gene is associated with acetylation of histones (H3 and H4) located in the 3′ untranslated region of the gene.[11] Histones bound to the β-myosin heavy chain gene have also been shown to be targeted by HATs in myocytes.[8]

Original received February 21, 2005; revision received June 1, 2005; accepted June 24, 2005.

From the Divisions of Functional Genomics (R.K., S.U., Y.Y., Y.L.C., K.K., S.T., T.W., H.M.) and Cardiovascular Medicine (R.K., S.U., K.S.), Jichi Medical School, Tochigi, Japan; and CREST (H.M.), Japan Science and Technology Agency, Saitama.

Correspondence to Dr Hiroyuki Mano, Division of Functional Genomics, Jichi Medical School, 3311-1 Yakushiji, Kawachigun, Tochigi 329-0498, Japan. E-mail hmano@jichi.ac.jp

Circulation Research **is available at http://circres.ahajournals.org** **DOI: 10.1161/01.RES.0000176028.18423.07**

We have recently established a new technique, differential chromatin scanning (DCS),[12] for genome-wide screening of DNA regions associated with histones that are differentially acetylated between a given pair of cell or tissue samples. To isolate target genes of HDACs in cardiac myocytes, we have now applied DCS to a rat embryonic heart–derived myogenic cell line, H9C2, treated or not with TSA. More than 200 genomic fragments were readily isolated by DCS, and genomic regions corresponding to 37 clones of 38 examined were confirmed to be associated with differentially acetylated histones. Furthermore, the expression of genes located in or close to such regions paralleled the associated level of histone acetylation.

Materials and Methods

Cell Culture

H9C2 cells were obtained from American Type Culture Collection (Rockville, Md) and were maintained in Dulbecco's modified Eagle's medium (DMEM; Invitrogen) supplemented with 10% fetal bovine serum (Invitrogen) and 2 mmol/L L-glutamine. For preparation of the tester sample, cells were incubated for 24 hours with 300 nM TSA (Wako). For other treatments, cells were incubated with 2 or 4 mmol/L sodium butyrate (Sigma) for 24 hours or with 1 nM cardiotrophin-1 (Calbiochemy) for the indicated times.

Neonatal cardiac myocytes were prepared as described previously.[13] In brief, ventricular tissue was dissected from newborn rats and subjected to digestion overnight at 4°C with trypsin (1 mg/mL; Invitrogen) in Hanks' balanced salt solution (Invitrogen). Myocytes were harvested by subsequent digestion of the tissue with collagenase (Worthington,) and were centrifuged twice at 50*g* to remove less dense cells such as fibroblasts. Myocytes were then cultured in DMEM-F12 (Invitrogen) supplemented with 10% fetal bovine serum and 2 mmol/L L-glutamine.

Differential Chromatin Scanning

HDAC targets were screened in H9C2 cells by DCS as described previously.[12] In brief, both tester and driver cells were fixed and subjected to immunoprecipitation with antibodies to acetylated histone H3 with the use of a chromatin immunoprecipitation (ChIP) assay kit (Upstate Biotechnology). DNA fragments recovered from the immunoprecipitates were digested with *Rsa*I (New England Biolabs), and the digestion products were ligated to the TAG adapter (5′-CCACCGCCATCCGAGCCTTTCTGCCCGGG-3′/3′-GAAAGACGGGCCC-5′). After polymerase chain reaction (PCR)–mediated amplification with the TAG primer (5′-CCACCGCCATCCGAGCCTTTCTGC-3′), the tester and driver DNA samples were digested with *Xma*I and *Sma*I, respectively. The tester DNA (0.5 μg) was ligated to the first subtraction adapter (5′-GTGAGGGTCGGATCTGGCTGGCTC-3′/3′-CGACCGAGGGCC-5′), annealed with 40 μg of the driver DNA at 67°C for 20 to 24 hours, and then subjected to PCR with the first subtraction primer (5′-GTGAGGGTCGGATCTGGCTGGCTC-3′). After digestion of single-stranded DNA with mung-bean nuclease (New England Biolabs), the amplified products were subjected to digestion with *Xma*I followed by a second round of subtraction PCR with the second subtraction adapter (5′-GTTAGCGGACACAGGGCGGGTCAC-3′/3′-GCCCAGTGGGCC-5′) and second subtraction primer (5′-GTTAGCGGACACAGGGCGGGTCAC-3′). The final products were digested with *Xma*I and ligated into pBlueScript (Stratagene). *Escherichia coli* DH5α cell clones transformed with the resulting recombinant plasmids were grown in 96-well plates and subjected to direct plasmid purification in the plates with the use of a Montage Plasmid Miniprep$_{96}$ Kit (Millipore). The nucleotide sequences of the purified plasmids were then determined by Dragon Genomics Center (Mie) and were used to screen, with the BLAT search program,[14] the nucleotide sequence database (http://genome.ucsc.edu/) assembled in June 2003 by the Genome Bioinformatics Group of the University of California at Santa Cruz (UCSC).

Quantitation of DNA

Genomic fragments immunoprecipitated by antibodies to acetylated histone H3 (Upstate Biotechnology) were subjected to PCR with a QuantiTect SYBR Green PCR Kit (Qiagen). The amplification protocol comprised incubations at 94°C for 15 s, 60°C for 30 s, and 72°C for 1 minute. Incorporation of the SYBR green dye into PCR products was monitored in real time with an ABI PRISM 7700 sequence detection system (PE Applied Biosystems), thereby allowing determination of the threshold cycle (C_T) at which exponential amplification of PCR products begins. The C_T values for DNA molecules in the immunoprecipitates and for those in the original sample before immunoprecipitation were used to calculate the abundance of the former relative to that of the latter. The oligonucleotide primers for PCR were 5′-CCGGAAGAGGTGGTTATGTAAA-3′ and 5′-GCTAAGAAGGGACAGGGCTAAC-3′ for the H9C2T-2_D09 clone, 5′-GTTTGTCTGGAGCCTGTACTCTC-3′ and 5′-AAGTTCTCCGTTTCAGGATTCAC-3′ for the H9C2T-2_C06 clone, 5′-CACATCCTTGGTGCTTCTGA-3′ and 5′-GAGGAGGGTGAGGAGCTGAG-3′ for the H9C2T-1_E03-1 clone, and 5′-CCCGGTGTTCTGTACGTAGG-3′ and 5′-ACTGATGGAGCATCCACATTCT-3′ for the H9C2T-S-1-8 clone.

Quantitation of mRNA

Total RNA was prepared from the tester and driver cells with an RNeasy Mini column (Qiagen) and was subjected to reverse transcription (RT) with PowerScript reverse transcriptase (BD Biosciences Clontech) and an oligo(dT) primer. Portions of the resulting cDNA were subjected to PCR with a QuantiTect SYBR Green PCR Kit. The amplification protocol comprised incubations at 94°C for 15 s, 60°C for 30 s, and 72°C for 1 minute. The C_T values for cDNAs corresponding to glyceraldehyde-3-phosphate dehydrogenase (GAPDH) mRNA and the mRNAs of interest were used to calculate the abundance of the latter relative to that of the former. The C_T values for GAPDH mRNA determined with 10 μg of total RNA from TSA-treated or nontreated cells were 18.5±0.8 and 18.2±0.2 (mean±SD), respectively, validating the use of GAPDH mRNA as an internal control.

The oligonucleotide primers for PCR were 5′-AATGTATCCGTTGTGGATCTGAC-3′ and 5′-ATTGTCATACCAGGAAATGAGCTT-3′ for GAPDH, 5′-GCCTGTGATACTCTGCTTATGTGT-3′ and 5′-CTTGAGGATTTCCTCTTTCTTCTG-3′ for the inositol 1,4,5-trisphosphate receptor type 3 gene (Itpr3), 5′-CAGTACCCTGTTGAGTCATCTCTG-3′ and 5′-GAAAGCAAGGTCTTCTTATTCTGG-3′ for the NAD(P)H dehydrogenase, quinone 1 gene (Nqo1), 5′-GCCTTCTACCTGCATACTACCAAG-3′ and 5′-AGTCTCAAGATACCGGAGCACA-3′ for the metastasis-associated 1 gene (Mta1), and 5′-CTGTTGGTACCTGTGCTGTGTAG-3′ and 5′-ACTGGTAGAGTACGTCCTTGTGG-3′ for the Jagged2 precursor gene (Jag2).

Statistical Analysis

Quantitation of DNA or mRNA was performed in triplicate in at least 2 independent experiments, and data are presented as mean±SD. The statistical significance of differences was analyzed by Student *t* test, with a probability value of <0.05 being considered significant.

Results

DCS in H9C2 Cells

Given that the ANP gene is a known target of HDAC in myocytes,[11] we first examined the effect of TSA on the acetylation level of histones bound to this gene in H9C2 cells. Real-time PCR analysis revealed that the amount of the 3′ untranslated region of the ANP gene that was precipitated by antibodies to acetylated histone H3 from TSA-treated cells was 7.85 times that precipitated from nontreated cells (data

not shown), indicating that the ANP gene is indeed a target of HDAC activity in H9C2 cells.

With the use of TSA-treated cells as the tester and nontreated cells as the driver, we then performed DCS, which in effect couples ChIP with subtraction PCR. After the second round of subtraction PCR, we sequenced the isolated genomic clones in a 96-well plate format. Analysis of 3 such plates thus yielded the nucleotide sequences of 288 DCS products. Among these randomly selected products, 222 clones contained >50 bp and were used to screen the nucleotide sequence database of UCSC with the use of the BLAT program.

A total of 195 clones showed >95% sequence identity to the rat genome sequence, and 178 of these clones were located either within protein-coding genes (demonstrated or predicted) or in the vicinity (within 10 kbp) of such genes (119 independent genes) (Table 1; Table SI available in the online supplement at http://circres.ahajournals.org). Forty-two (23.6%) of the 178 clones were assigned to a region spanning the promoter (0 to −2000 bp relative to the transcriptional start site), the first exon, and the first intron of the corresponding genes. Given that protein-coding genes account for only a few percent of the rat genome,[15] our data suggest that histone acetylation occurs preferentially at regions of the genome involved directly in transcriptional regulation.

Eleven DCS clones were assigned to overlapping sequences upstream of the Oct11 gene, and 7 clones were mapped to overlapping sequences at chromosomal position 8q24, a region with no annotation information (data not shown). The isolation of such multiple clones for individual genomic regions suggests that the DCS products isolated may represent most HDAC targets in H9C2 cells.

HDAC Targets in a Cardiomyocyte Cell Line

To verify the fidelity of DCS, we randomly selected 38 DCS clones and quantified the corresponding genomic fragments in immunoprecipitates prepared from both tester and driver cells with antibodies to acetylated histone H3. The amount of each DNA fragment in the immunoprecipitate relative to that in the original sample before ChIP was determined by real-time PCR. Selective amplification by DCS proved to be highly reliable (Table 1), with 37 of the 38 clones exhibiting tester-selective precipitation (tester/driver ratio of ≥1.5). It is therefore likely that DCS indeed identified targets of HDAC in myocytes.

To visualize directly the genome-wide distribution of HDAC targets, we mapped to rat chromosome figure our genomic clones whose chromosomal positions were known (Figure 1). The HDAC targets were distributed widely throughout the rat genome, although some "hot spots" for deacetylation were apparent. For example, 7 of the DCS clones mapped to chromosomal position 5q36, and detailed mapping revealed that all of these clones were located within a region spanning 27 Mbp. It is thus possible that regional alterations of chromatin structure result in coordinated transcriptional regulation of genes within the affected region.

Some of the clones listed in Table 1 correspond to loci within or close to rat genes whose products function in intracellular calcium mobilization or antioxidant processes. One such clone (H9C2T-2_D09), for instance, mapped to a region encompassing intron 21 and exon 22 of Itpr3 (Figure 2A), which encodes a receptor for inositol 1,4,5-trisphosphate that plays an important role in Ca^{2+}-mediated signal transduction. The cytosolic concentration of Ca^{2+} directly regulates muscle contraction and cardiac rhythm and is a determinant of myocyte hypertrophy and heart failure.[16] The amount of the genomic fragment corresponding to the H9C2T-2_D09 clone was 6.6-fold greater in the ChIP product of TSA-treated cells than in that of untreated cells (Figure 2B), indicating that the extent of histone acetylation in this region of the genome of the tester cells was 6.6 times that in the driver cells. Furthermore, inhibition of HDAC activity was accompanied by an increase in the amount of Itpr3 mRNA (Figure 2C). These data suggest that HDAC actively deacetylates a chromosomal region corresponding to Itpr3 and thereby suppresses the transcriptional activity of the gene.

Another clone (H9C2T-2_C06) was mapped to the first intron of Nqo1 (Figure 2D), which encodes a reductase that contributes to detoxification of quinones and to regulation of apoptosis.[17] We examined whether the acetylation of associated histones and the expression of Nqo1 are regulated by HDAC activity in cardiomyocytes. As with Itpr3, the acetylation level of histones bound to Nqo1 was increased by TSA treatment in H9C2 cells (Figure 2E), and this epigenetic change was accompanied by an increase in the amount of Nqo1 mRNA (Figure 2F).

Nineteen (10.7%) of the 178 clones whose chromosomal location was known were assigned to loci corresponding to at least 2 genes in the rat genome. One such clone, H9C2T-1_E03-1, was mapped to a region corresponding to the first intron of Mta1 and to the last exon of Jag2 (Figure 3A). Histone acetylation in this region might thus affect the transcription of both genes simultaneously. The level of histone H3 acetylation in this region was confirmed to be greater in the tester cells than in the driver cells (Figure 3B). However, although inhibition of HDAC activity by TSA resulted in upregulation of the amount of Jag2 mRNA (Figure 3C), it had no effect on the abundance of Mta1 mRNA (Figure 3D). Histone acetylation in the genomic region that encompasses both Jag2 and Mta1 thus appears to regulate the transcriptional activity of the former gene but not that of the latter. Jag2 is a ligand for the receptor Notch1 and is abundant in the heart.[18] Coculture of fibroblasts expressing human JAG2 with murine C2C12 myoblasts resulted in inhibition of myogenic differentiation of the latter cells, implicating JAG2 in regulation of this process.

We selected an additional 19 DCS clones for quantitation of the corresponding mRNAs. Among the genes examined, 6 were preferentially expressed (tester/driver ratio of ≥1.5) in the TSA-treated cells compared with the nontreated cells (Table 1).

Regulation of Histone Acetylation in Neonatal Rat Cardiac Myocytes

Our DCS analysis identified HDAC targets in a cardiomyocyte cell line. To investigate whether the level of histone

Fragments of the Rat Genome Isolated by DCS in H9C2 Cells

Clone ID	Tester/Driver DNA Ratio	Annotation	GenBank Accession No. (or Ensemble Gene ID)	Locus	Tester/Driver mRNA Ratio	Position Relative to Corresponding Genes
H9C2T-S-2–8	13.7	EST	BQ204614	19q12	5.34	Intron 2
H9C2T-S-1-5b	10.92	Skn-1a	L23862	8q22		4 kbp upstream of exon 1
H9C2T-1_D09	10.7	Putative G protein–coupled receptor (SENR) gene (Senr)	NM_020537	10q32.3	1.09×10^{8}	Exon 1
H9C2T-S-1-2b	9.36	NA	NA	20p12		
H9C2T-1_B05	8.43	No description	(ENSRNOG00000013959)	8q24		Last exon+last intron
H9C2T-S-1-8	7.96	Myocilin (Myoc)	NM_030865	13q22	2.03	2.5 kbp upstream of exon 1
H9C2T-1_E03-1*	7.85	Mta1 (mta1)	NM_022588	6q32	0.91	Intron 1
		Jagged2 precursor	U70050		8.43	Last exon
H9C2T-2_E05	7.7	Protein kinase C and casein kinase substrate in neurons 1 (Pacsin1)	NM_017294	20p12	26.45	Intron 1
H9C2T-1_C04-2	7.69	Carbohydrate (chondroitin 6/keratan) sulfotransferase 3 (Chst3)	NM_053408	20q11	0.25	Intron 1
H9C2T-S-1-2a	6.99	Phosphodiesterase	L27061	16p14	1.12×10^{8}	1.3 kbp upstream of exon 1
H9C2T-S-1-4	6.76	EST	CB741111	14p22		Intron 3
H9C2T-S-1-5a	6.64	Brain and reproductive organ–expressed protein	NM_199270	6q13		Intron 10
H9C2T-1_C04-1	6.61	EST	CO562897	3q43		Exon 1
H9C2T-2_D09	6.6	Inositol 1,4,5-trisphosphate receptor 3 (Itpr3)	NM_013138	20p12	1.66	Intron 21+exon 22
H9C2T-2_E11	6.51	EST	CV077786	3q43		Last exon
H9C2T-1_H05-1	6.29	Microtubule-associated protein tau (Mapt)	NM_017212	10q32.1	602.17	Intron 7
H9C2T-1_G12	5.83	No description	(ENSRNOG00000004217)	10q12		Intron 2
H9C2T-1_H01	5.36	A disintegrin and metalloproteinase domain 1 (fertilin alpha) (Adam1)	NM_020078	12q16	0.46	Last intron
H9C2T-2_F10-1	5.13	Translocase of outer mitochondrial membrane 20 homolog (yeast) (Tomm20)	NM_152935	19q12		Last intron
H9C2T-S-1-7	5.06	EST	BF282351	4q34	0.68	2 kbp upstream of exon 1
H9C2T-1_H10	4.92	Collagen, type V, alpha 1 (Col5a1)	NM_134452	3p12	0.86	Intron 1
H9C2T-2_H07	4.4	Runt-related transcription factor 1 (Runx1)	NM_017325	11q11	1.21	Intron 4
H9C2T-S-1-3	4.36	No description	(ENSRNOG00000021887)	8q32		Last exon+last intron
H9C2T-S-2-3	4.35	EST	CO557128	1q43		0.5 kbp upstream of exon 1
H9C2T-2_A01′	3.9	Fos-like antigen 1 (Fosl1)	NM_012953	1q43	0.39	1 kbp downstream of last exon
H9C2T-S-2-7	3.86	Arylsulfatase B (ARSB)	D49434	2q12	0.48	Intron 4
H9C2T-1_F10	3.85	Phosphatidylinositol 4-kinase (Pik4cb)	NM_031083	2q34	0.88	Exon 4
H9C2T-2_C06	3.78	NAD(P)H dehydrogenase, quinone 1 (Nqo1)	NM_017000	19q12	2.82	Intron 1
H9C2T-1_D03	3.79	Cytokine-inducible SH2-containing protein	AF065161	8q32	1.47	Last exon
H9C2T-1_F09-1*	3.74	EST	CK597511	15p16		Immediately upstream of exon 1
		Normalized rat muscle, Bento Soares Rattus sp. cDNA clone RMUBG18 3′ end	AI171102			Intron 1
		EST	CK598708			Exon 1
H9C2T-2_B07	3.62	Cyclin D1 (Ccnd1)	NM_171992	1q42	0.59	Intron 3+exon 4
H9C2T-1_C03-1	3.58	G protein beta subunit–like (Gbl)	NM_022404	10q12	0.77	Last exon
H9C2T-2_A11	3.4	EST	CO557128	1q43		0.5 kbp upstream of exon 1
H9C2T-S-2-1	3.37	Period1 (rper1), partial cds	AB092976	10q24	0.52	Introns 15, 16+exon 16
H9C2T-2_E03-2	2.94	Interleukin-11 (Il11)	NM_133519	1q12	1	Intron 5
H9C2T-S-1-1	2.69	No description	(ENSRNOG00000001730)	11q22		Intron 3
H9C2T-1_C09	1.83	No description	(ENSRNOG00000025448)	10q32.1		0.5 kbp upstream of exon 1

EST indicates expressed sequence tag; NA, not assigned. *Fragments that mapped to loci of multiple genes.

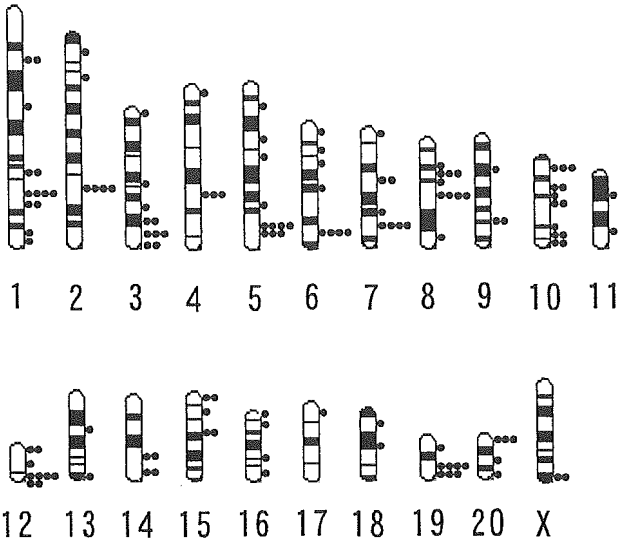

Figure 1. Chromosomal distribution of HDAC targets in rat cardiomyocytes. Genomic fragments (red dots) isolated by DCS were mapped to rat chromosomes.

acetylation at these targets is also affected by HDAC activity in differentiated cardiomyocytes, we isolated cardiac myocytes from neonatal rats and incubated these cells in the absence or presence of TSA. Consistent with the results obtained with H9C2 cells (Figures 2 and 3), TSA treatment resulted in marked increases both in the acetylation level of histones associated with the genomic locus corresponding to clone H9C2T-2_D09 and in the amount of Itpr3 mRNA in neonatal rat cardiac myocytes (Figure 4A). Similarly, TSA increased both the histone acetylation level for genomic DNA corresponding to clone H9C2T-2_C06 and the abundance of Nqo1 mRNA in the rat cardiac myocytes (Figure 4B). Furthermore, TSA increased the level of histone acetylation associated with the genomic locus corresponding to clone H9C2T-1_E03-1 in rat cardiac myocytes and, as in H9C2 cells, it increased the amount of Jag2 mRNA without affecting that of Mta1 mRNA (Figure 4C). Quantitation of genomic DNA corresponding to an additional 19 DCS clones in ChIP products prepared from neonatal rat cardiac myocytes revealed that the acetylation level of bound histones was increased by a factor of >5 by TSA treatment (data not shown). These data thus indicate that the genomic clones identified by DCS in H9C2 cells represent genomic regions whose associated histones are targeted by HDAC activity in differentiated cardiac myocytes. Twelve of the 23 genes that mapped to (or in the vicinity of) the DCS clones examined were also transcriptionally activated by a factor of >1.5 in the TSA-treated neonatal rat cardiac myocytes compared with nontreated cells (data not shown).

Effects of Sodium Butyrate on Histone Acetylation

Various compounds other than TSA inhibit HDAC activity with different target preferences.[19] Sodium butyrate, for example, inhibits the catalytic activity of HDACs belonging to class I or IIA, whereas TSA inhibits that of HDACs belonging to class I, IIA, or IIB. We therefore examined

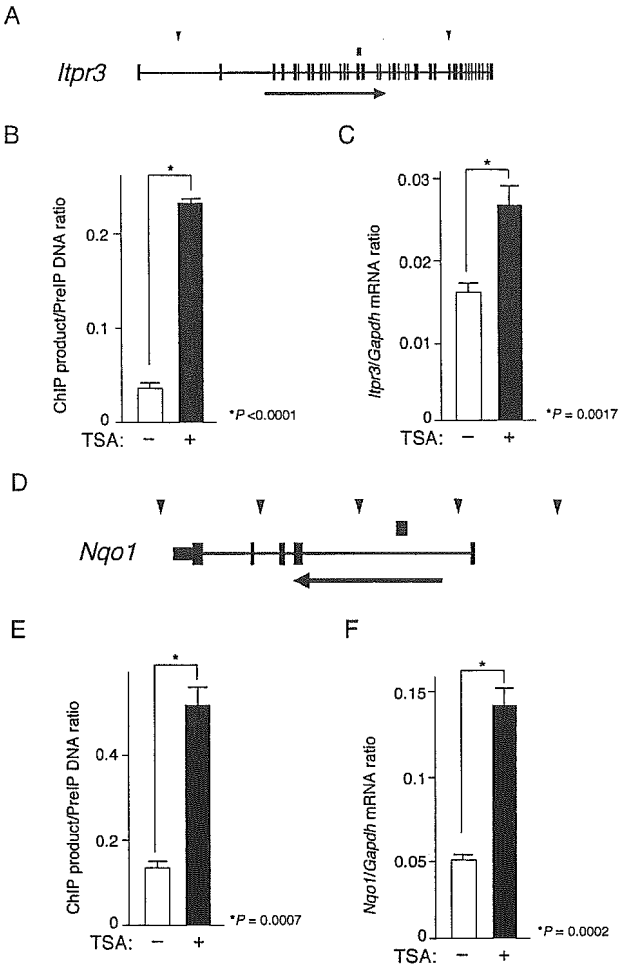

Figure 2. Identification of Itpr3 and Nqo1 as targets of HDAC in cardiomyocytes. A, One of the DCS clones (H9C2T-2_D09; red rectangle) was mapped to chromosome 20p12, spanning intron 21 and exon 22 of Itpr3. Exons are denoted by black boxes, the arrow indicates the direction of transcription, and blue triangles depict distance markers separated by 50 kbp. B, Chromatin immunoprecipitates were prepared from H9C2 cells treated (+) or not (−) with 300 nM TSA for 24 hours. The amount of DNA corresponding to the H9C2T-2_D09 sequence in each ChIP product relative to that in the corresponding original sample before immunoprecipitation (PreIP) was then determined by real-time PCR. C, The amount of Itpr3 mRNA relative to that of GAPDH mRNA in H9C2 cells treated or not with TSA was determined by quantitative RT-PCR. D, One of the DCS clones (H9C2T-2_C06; red rectangle) was mapped to chromosome 19q12 in the first intron of Nqo1. Green triangles depict distance markers separated by 5 kbp. E, The amount of genomic DNA corresponding to the H9C2T-2_C06 sequence in ChIP products relative to that in the PreIP samples was measured as in B. F, The amount of Nqo1 mRNA relative to that of GAPDH mRNA was determined as in C. All data are mean±SD of triplicates from representative experiments that were performed at least twice. Probability values for the indicated comparisons were determined by Student *t* test.

whether sodium butyrate also affects the acetylation level of histones associated with our DCS clones.

H9C2 cells or neonatal rat cardiac myocytes were incubated for 24 hours with 0, 2, or 4 mmol/L sodium butyrate and then subjected to ChIP, and the resulting products were subjected to real-time PCR to quantitate the amount of genomic DNA corresponding to the clones

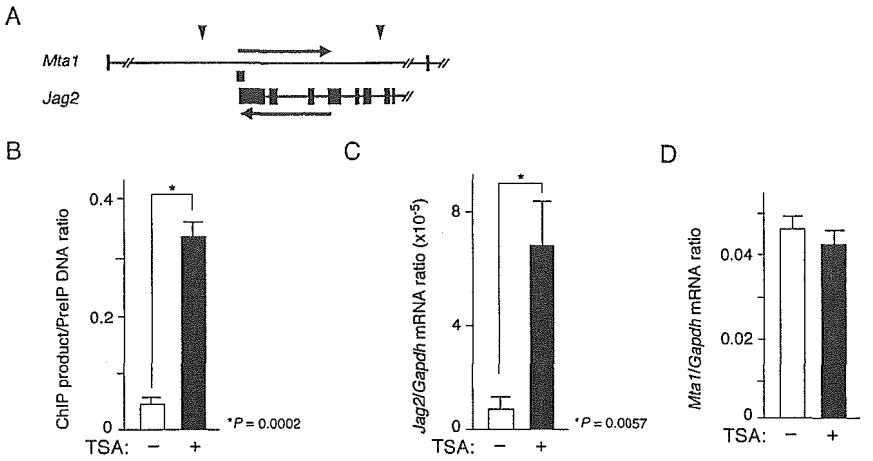

Figure 3. Identification of Mta1 and Jag2 as targets of HDAC in cardiomyocytes. A, One of the DCS clones (H9C2T-1_E03-1; red rectangle) was mapped to chromosome 6q32 in the first intron of Mta1 and the last exon of Jag2. The position of the H9C2T-1_E03-1 clone in the genome is shown schematically as in Figure 2D. B, The amount of genomic DNA corresponding to the H9C2T-1_E03-1 sequence in ChIP products relative to that in the PreIP samples was measured by real-time PCR as in Figure 2B. C and D, The amounts of Jag2 (C) and Mta1 (D) mRNAs relative to that of GAPDH mRNA were determined as in Figure 2C. All data are mean±SD of triplicates from representative experiments, and probability values for the indicated comparisons were determined by Student *t* test.

H9C2T-2_D09, H9C2T-2_C06, or H9C2T-1_E03-1. Treatment with sodium butyrate at either 2 or 4 mmol/L resulted in marked increases in the amount of DNA corresponding to each clone in the ChIP products from both H9C2 cells (Figure 5A) and neonatal rat cardiac myocytes (Figure 5B). Although the magnitudes of the effects of 2 and 4 mmol/L sodium butyrate were similar in H9C2 cells, the effects of the higher concentration were greater than those of the lower concentration in the differentiated cardiac myocytes. The genomic regions corresponding to these 3 DCS clones were thus epigenetically regulated by both TSA and sodium butyrate.

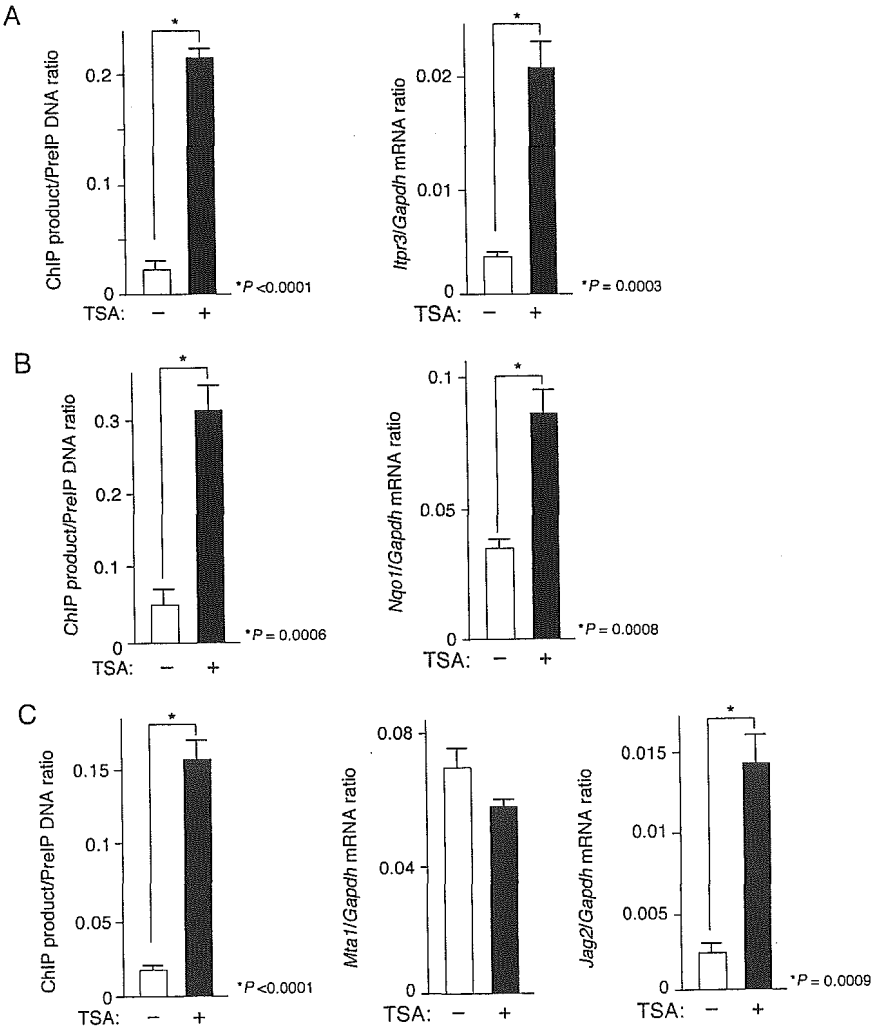

Figure 4. Histone acetylation status and gene expression in neonatal rat cardiac myocytes. Chromatin immunoprecipitates were prepared from freshly isolated cardiac myocytes treated (+) or not (–) with 300 nM TSA for 24 hours, and the amount of DNA corresponding to the H9C2T-2_D09 (A), H9C2T-2_C06 (B), or H9C2T-1_E03-1 (C) clones in each ChIP product was determined by real-time PCR. The amount of Itpr3 (A), Nqo1 (B), or Mta1 and Jag2 (C) mRNAs in cells treated or not with TSA was determined by quantitative RT-PCR. All data are mean±SD of triplicates from representative experiments, and probability values for the indicated comparisons were determined by Student *t* test.

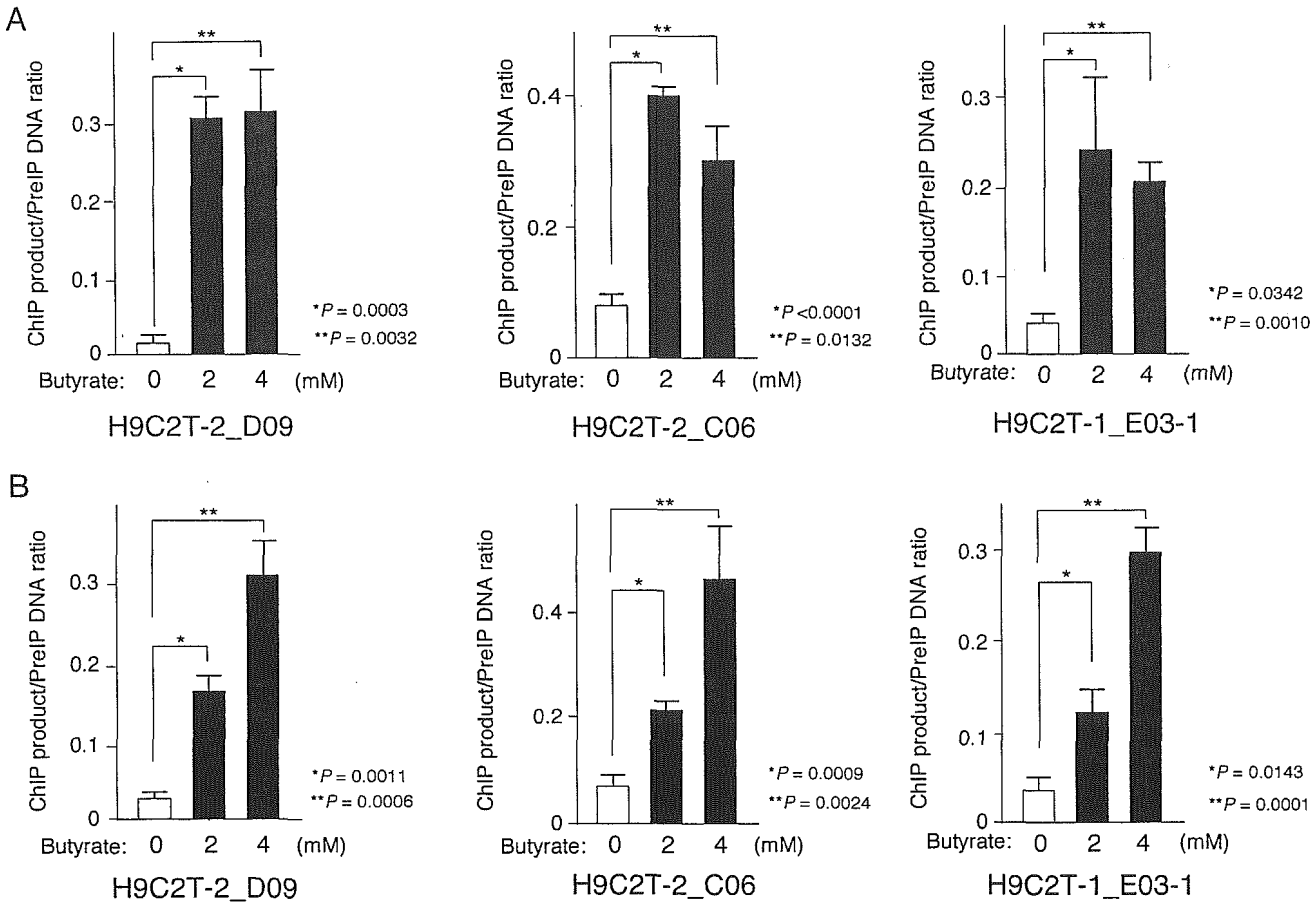

Figure 5. Regulation of histone acetylation status by sodium butyrate. Chromatin immunoprecipitates were prepared from H9C2 cells (A) or freshly isolated rat neonatal cardiac myocytes (B) after treatment with 0, 2, or 4 mmol/L sodium butyrate for 24 hours, and the amount of DNA corresponding to the H9C2T-2_D09, H9C2T-2_C06, or H9C2T-1_E03-1 clones in each ChIP product was determined. All data are mean±SD of triplicates from representative experiments, and probability values for the indicated comparisons were determined by Student *t* test.

Regulation of HDAC Targets by a Hypertrophic Stimulus

Given that H9C2 cells retain the ability to undergo hypertrophic changes in response to various stimuli,[20,21] we next examined whether stimulation with a physiological hypertrophic agent, cardiotrophin-1 (CT-1), affects the extent of histone acetylation at genomic regions corresponding to DCS clones in these cells. H9C2 cells were incubated with 1 nM CT-1 for various times up to 24 hours and were then subjected to ChIP and real-time PCR analysis. Quantitation of genomic DNA revealed that the level of histone acetylation at the region corresponding to clone H9C2T-1_E03-1 was increased significantly at 6 hours and was still increasing at 24 hours (Figure 6A). Similar to the effects of TSA at this locus (Figure 3), the increase in histone acetylation induced by CT-1 was not accompanied by a change in the amount of Mta1 mRNA (Figure 6B), but was associated with a transient activation of Jag2 transcription apparent after stimulation for 6 hours (Figure 6C).

Finally, we analyzed a different DCS clone for epigenetic regulation by CT-1. The H9C2T-S-1-8 clone corresponds to the promoter region for the Myocilin (Myoc) gene (Figure 6D). This gene encodes a protein involved in cytoskeletal function, and mutations in Myoc have been shown to cause a hereditary form of juvenile-onset open-angle glaucoma.[22] We found that CT-1 induced a time-dependent increase in the extent of histone acetylation at the genomic region corresponding to this DCS clone (Figure 6E). Together, these data indicate that the histone acetylation level of genomic regions corresponding to our DCS clones is regulated not only by TSA and sodium butyrate but also by physiological stimuli.

Discussion

With the use of our recently developed screening method, DCS, we have now identified almost 200 HDAC targets in cardiomyocytes. The acetylation of histones associated with genomic regions corresponding to 37 of 38 randomly chosen DCS clones was confirmed to be induced by treatment of H9C2 cells with TSA. Genomic regions corresponding to DCS clones were also epigenetically regulated by another HDAC inhibitor, sodium butyrate. Furthermore, the histone acetylation level of genomic regions corresponding to all 22 DCS clones examined was shown to be HDAC targets also in freshly isolated cardiac myocytes. Finally, the acetylation level of histones associated with DCS clones was shown to be regulated by a physiological stimulus, CT-1. The genomic

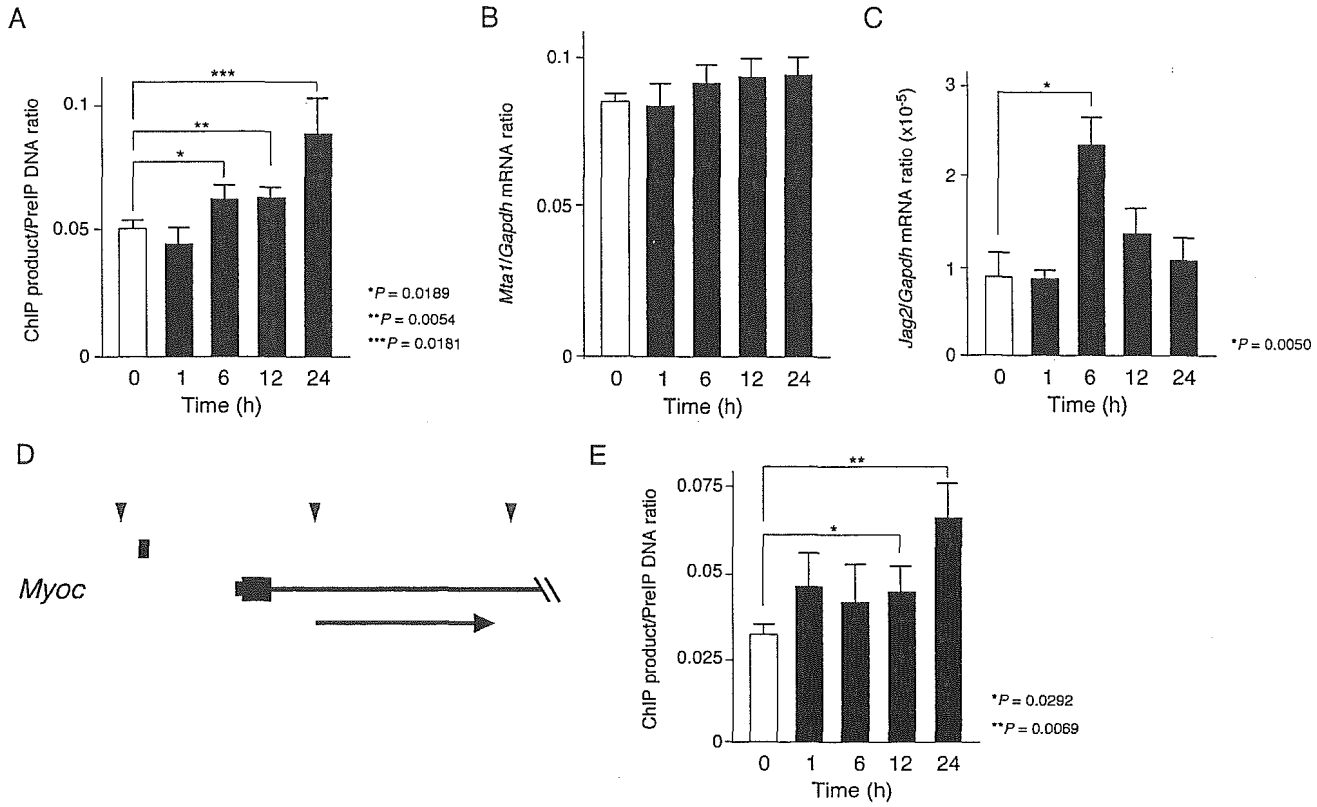

Figure 6. Effects of CT-1 on histone acetylation in H9C2 cells. A, H9C2 cells stimulated with CT-1 (1 nM) for the indicated times were subjected to ChIP, and the amount of genomic DNA corresponding to the DCS clone H9C2T-1_E03-1 was determined in ChIP products. B and C, The amounts of Mta1 (B) and Jag2 (C) mRNAs relative to that of GAPDH mRNA were determined by quantitative RT-PCR in H9C2 cells stimulated with CT-1 for the indicated times. D, The H9C2T-S-1-8 clone (red rectangle) was mapped to chromosome 13q22 in the promoter region of Myoc. The position of the clone in the genome is shown schematically as in Figure 2D. E, The amount of genomic DNA corresponding to the H9C2T-S-1-8 sequence was determined in ChIP products prepared from H9C2 cells treated with CT-1 for the indicated times. All data are mean±SD of triplicates from representative experiments, and probability values for the indicated comparisons were determined by Student *t* test.

loci identified by DCS thus include physiologically relevant targets for epigenetic modification.

The HDAC targets identified in cardiomyocytes include several genes related to cell growth or differentiation that might play an important role in heart function. In addition to Itpr3 and Jag2, such genes include those for G protein–coupled receptors (Senr, Gbl), regulators of cytosolic Ca^{2+} concentration (phosphodiesterase, Pik4cb, Pacsin1), and mediators of growth signaling (Ccnd1, Runx1, Fosl1, Il11, Oct11, Sox6) (online Table SI). Our data suggest that these various genes are under epigenetic control in cardiomyocytes, a conclusion that was verified for some of them by the demonstration that the level of acetylation of associated histones was regulated by the physiological stimulus CT-1. Although CT-1 has not previously been shown to elicit intracellular signaling that affects histone acetylation, our data now indicate that this is indeed the case.

Many (42 of 178) of our DCS clones mapped to the 5′-regions of genes in the rat genome. Bernstein et al recently attempted to identify loci in the human genome whose associated histones are acetylated.[23] These researchers used the "ChIP on chip"[24] strategy with high-density genome-tilling microarrays for human chromosomes 21 and 22. Interestingly, consistent with our results, they found that histone H3 acetylated on lysine-9 and lysine-14 was preferentially localized at the 5′ ends of genes, with 58% of such sites of histone acetylation residing in regions encompassing −1.0 to +1.0 kbp of known genes.

Acetylation of core histones is not always associated with the regulation of gene transcription, however. Histone acetylation may thus be related to chromosome replication or to chromatin remodeling unrelated to transcriptional regulation.[25] In addition, various types of covalent modification, including acetylation, phosphorylation, and methylation, may exert their effects on histones in a coordinated manner, resulting in the generation of a so-called histone code.[26] Consistent with these considerations, only 39% and 52% of the genes corresponding to DCS clones examined showed preferential expression in TSA-treated H9C2 cells and TSA-treated neonatal rat cardiac myocytes, respectively, compared with the corresponding untreated cells.

Although DCS does not readily allow a quantitative comparison of the level of histone acetylation between samples, our method is technically straightforward and does not require any specialized apparatus such as a DNA microarray system. In conclusion, DCS enabled us to efficiently identify HDAC targets in cardiomyocytes. Our present data support the feasibility of determining genome-wide histone acetyla-